

β 1-Integrin- and K_v 1.3 channel-dependent signaling stimulates glutamate release from Th17 cells

Katharina Birkner,¹ Beatrice Wasser,¹ Tobias Ruck,² Carine Thalman,¹ Dirk Luchtman,¹ Katrin Pape,¹ Samantha Schmaul,¹ Lynn Bitar,¹ Eva-Maria Krämer-Albers,³ Albrecht Strohm,⁴ Sven G. Meuth,² Frauke Zipp,¹ and Stefan Bittner¹

¹Department of Neurology, Focus Program Translational Neuroscience (FTN) and Immunotherapy (FZI), Rhine Main Neuroscience Network (rmn²), University Medical Center of the Johannes Gutenberg University Mainz, Mainz, Germany. ²Department of Neurology, University of Muenster, Muenster, Germany. ³Institute for Molecular Cell Biology, Johannes Gutenberg University Mainz, Mainz, Germany.

⁴Institute for Pathophysiology, FTN, University Medical Center of the Johannes Gutenberg University Mainz, Mainz, Germany.

Although the impact of Th17 cells on autoimmunity is undisputable, their pathogenic effector mechanism is still enigmatic. We discovered soluble N-ethylmaleimide-sensitive factor attachment receptor (SNARE) complex proteins in Th17 cells that enable a vesicular glutamate release pathway that induces local intracytoplasmic calcium release and subsequent damage in neurons. This pathway is glutamine dependent and triggered by binding of β 1-integrin to vascular cell adhesion molecule 1 (VCAM-1) on neurons in the inflammatory context. Glutamate secretion could be blocked by inhibiting either glutaminase or K_v 1.3 channels, which are known to be linked to integrin expression and highly expressed on stimulated T cells. Although K_v 1.3 is not expressed in CNS tissue, intrathecal administration of a K_v 1.3 channel blocker or a glutaminase inhibitor ameliorated disability in experimental neuroinflammation. In humans, T cells from patients with multiple sclerosis secreted higher levels of glutamate, and cerebrospinal fluid glutamine levels were increased. Altogether, our findings demonstrate that β 1-integrin- and K_v 1.3 channel-dependent signaling stimulates glutamate release from Th17 cells upon direct cell-cell contact between Th17 cells and neurons.

Introduction

Glutamate is an essential excitatory neurotransmitter in the CNS, but excessive glutamate concentrations can be harmful, inducing excitotoxicity and massive loss of brain function (1–3). It has been suggested that in patients with multiple sclerosis (MS), extracellular accumulation of glutamate leads to direct toxic effects on neurons (4) via an AMPA receptor-dependent (and probably also an NMDA receptor-dependent), long-lasting increase in intracellular Ca^{2+} concentrations (5). Although the source of glutamate is not known, direct proof in humans is lacking, and the underlying pathway is not understood. Imaging-based approaches (MR spectroscopy) are currently not capable of differentiating intracellular stores from extracellularly located glutamate relevant for excitotoxic effector mechanisms (4). Yet, it was demonstrated in animal models and cerebrospinal fluid (CSF) of patients with MS that extracellular glutamate increases up to approximately 100 μ M compared with basal levels of approximately 5 μ M in healthy donors (6, 7). Treatment with glutamatergic antagonists diminishes neurological deficits and axonal degeneration in animal models of MS. However, available broad antiglutamatergic drugs such as amantadine, memantine, and riluzole (4) are associated with side effects that limit their use and underline the need to understand how glutamate contributes to immune-mediated white and gray matter damage in MS

(8, 9). To date, some groups have found that T lymphocytes themselves are able to secrete glutamate (10–12). Interestingly, as the most abundant amino acid in the bloodstream, glutamine has also been implicated as an immunomodulatory nutrient (13). Recent studies showed that glutamine drives the differentiation of naive $CD4^+$ cells into inflammatory Th17 cells but not into Th2 cells or Tregs (14–16). However, the underlying role of glutamine/glutamate pathways in CNS inflammation remains unclear.

Th17 cells infiltrating the CNS play a crucial role in MS and its animal model experimental autoimmune encephalomyelitis (EAE) (17–19). Moreover, Th17 cells have been proposed as a driving force in autoimmune neuroinflammation (20–22), as they can destabilize the blood-brain barrier, secrete proinflammatory cytokines (23), and recruit immune cells to the CNS, thereby orchestrating a proinflammatory environment (24, 25). Furthermore, we previously demonstrated that Th17 cells can induce intracellular Ca^{2+} elevations in neurons via a direct cell-cell contact-dependent mechanism (12). Neuronal Ca^{2+} elevations can either lead to axonal swelling and cell death or to a transient state enabling recovery (12, 26). However, the role of Th17 cells in CNS damage is far from being unraveled, and the link to neuronal injury is questioned (27–29).

Here, we show that Th17 cells depend on external glutamine supply to secrete the excitatory neurotransmitter glutamate in a time-dependent and T cell receptor-dependent (TCR-dependent) manner. In contrast to Th1 cells, Th17 cells possess the molecular machinery for Ca^{2+} -dependent vesicular glutamate release, which can be blocked in vitro and in vivo by inhibiting the K_v 1.3 channel (KCNA3) or glutaminase. K_v 1.3 is highly expressed on stimulated T cells and has been linked to integrin expression. In an inflammatory context, binding of Th17 cells to neurons that upregulate

Authorship note: FZ and SB contributed equally to this work.

Conflict of interest: The authors have declared that no conflict of interest exists.

Copyright: © 2020, American Society for Clinical Investigation.

Submitted: November 26, 2018; **Accepted:** October 22, 2019; **Published:** January 6, 2020.

Reference information: *J Clin Invest.* 2020;130(2):715–732.

<https://doi.org/10.1172/JCI126381>.

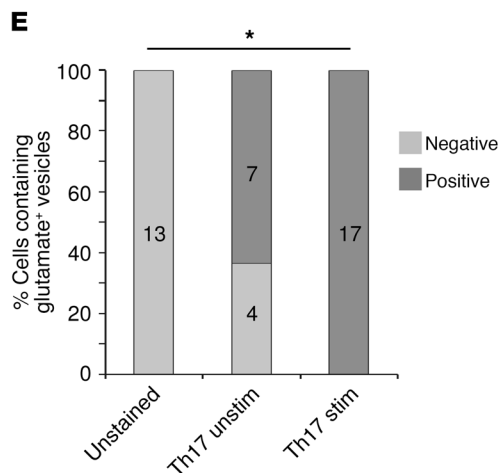
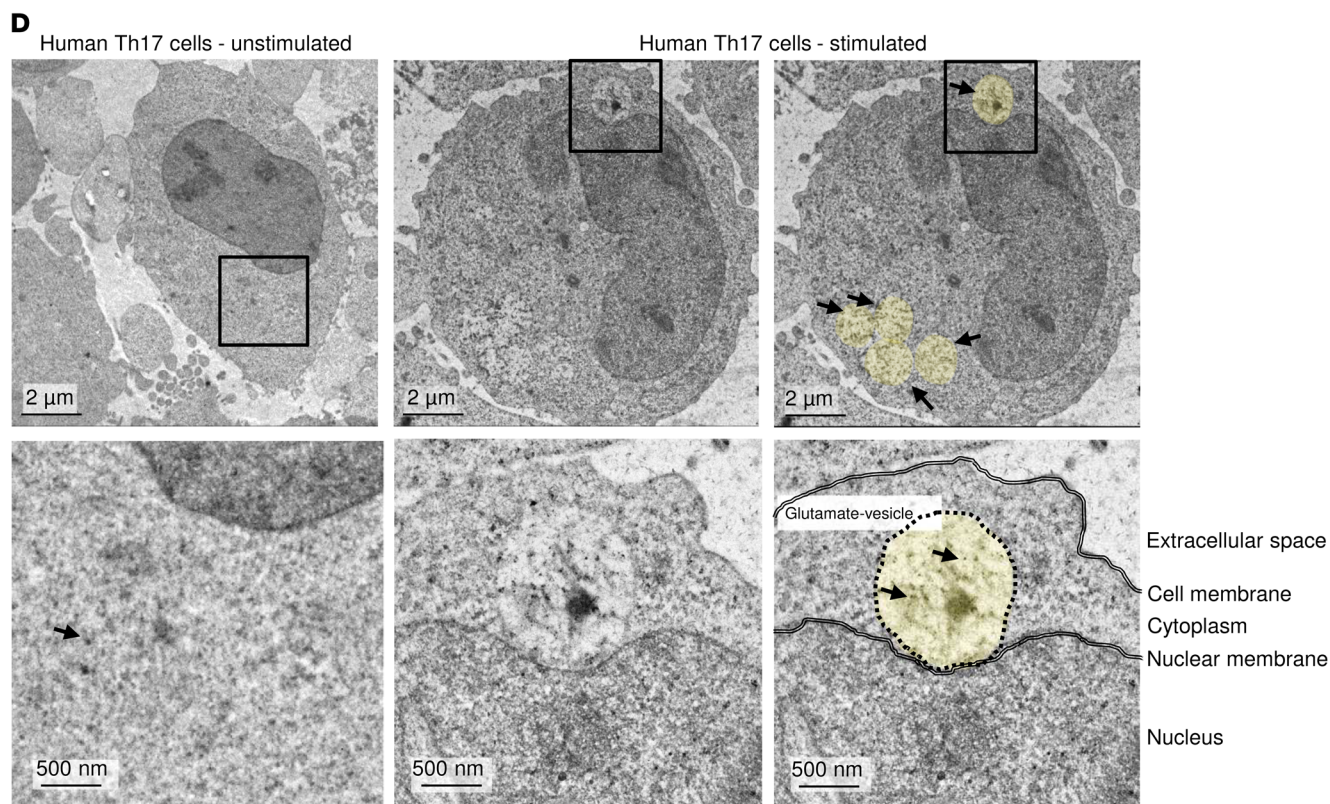
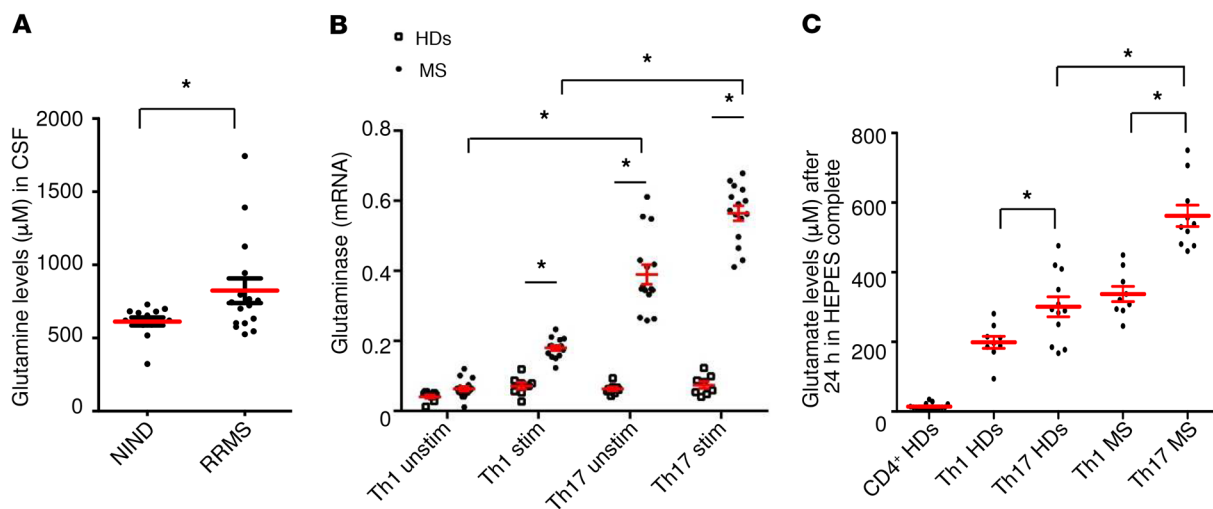


Figure 1. Patients with MS have higher glutamine levels in the CSF and elevated glutamate secretion by T cells. (A) Glutamine levels were assessed in the CSF of patients with RRMS ($n = 16$) or noninflammatory neurological disease (NIND) ($n = 14$). (B) mRNA analysis of the enzyme glutaminase was performed in unstimulated and stimulated human Th1 and Th17 cells from 8 healthy donors (HDs) and 15 patients with MS after 24 hours (normalized to β -actin). (C) Human CD4⁺ cells were isolated from PBMCs of healthy donors ($n = 17$), and glutamate levels were measured after 24 hours. In another set of experiments, differentiated Th1 and Th17 cells from healthy donors ($n = 6$) and patients with MS ($n = 7$) were compared. (D) Post-embedding immunogold labeling of fixed L-glutamate was measured with an electron microscope. Unstimulated human Th17 cells showed only sporadic positive signals in the cytoplasm (left panels), whereas stimulated human Th17 cells showed clear positive signals in the cytoplasm and in vesicles (middle and right panels). Yellow circles highlight vesicular structures; black arrows indicate glutamate. Scale bars: 2 μ m and 500 nm. (E) Quantification of glutamate-positive cells within unstained ($n = 13$), unstimulated (Th17 unstim) ($n = 11$), and stimulated (Th17 stim) ($n = 17$) human Th17 cells. Data indicate the mean \pm SEM. * $P < 0.05$, by unpaired Student's t test (A), 1-way ANOVA with Tukey's post hoc test (B and C), or χ^2 test (E).

vascular cell adhesion molecule 1 (VCAM-1) via β 1-integrin (CD29) was identified as the trigger for glutamate release. In humans, Th17 cells from patients with MS secreted higher glutamate levels than did cells from healthy donors; glutamine levels in the CSF as well as glutaminase mRNA expression levels in Th17 cells were also elevated in patients with MS, underlining the pathological relevance of this newly identified detrimental effector pathway.

Results

Patients with MS have elevated glutamine levels in the CSF, and T cells from patients with MS secrete higher levels of glutamate. To investigate the relevance of T cell-mediated glutamate release in humans, we first assessed the levels of glutamine, which can be metabolized to glutamate by the enzyme glutaminase in the CSF. Patients with MS had elevated glutamine levels in the CSF compared with patients with noninflammatory neurological diseases (Figure 1A and Supplemental Table 1; supplemental material available online with this article; <https://doi.org/10.1172/JCI126381DS1>). Glutaminase levels were significantly higher in unstimulated and stimulated Th17 cells from patients with MS than in Th1 cells or than in Th17 cells from healthy donors, indicating a high capacity for glutamate production (Figure 1, B and C). Indeed, the polarization of memory CD4⁺CD45RO⁺ cells into Th17 cells strongly increased glutamate secretion in comparison with undifferentiated human CD4⁺ cells. Moreover, Th17 cells derived from patients with MS secreted significantly higher levels of glutamate than did Th1 or Th17 cells derived from healthy donors (Figure 1C), whereas T effector functions such as IL-17 production did not differ (Supplemental Figure 1A). Cytokine production and transcription factor expression clearly differentiated human Th1- and Th17-polarized cells (Supplemental Figure 1, B-D). Using electron microscopy with immunogold labeling of fixed glutamate, we observed that stimulated Th17 cells had positive signals in the cytoplasm and within newly formed vesicles, whereas unstimulated human Th17 cells contained fewer glutamate-positive vesicles. We detected no positive signals in the unstained control cells (Figure 1, D and E).

Th17 cells possess the molecular machinery for vesicular glutamate release as a pathway of T cell-mediated neuronal excitotoxicity. We next addressed how glutamate secretion is regulated in polarized murine Th17 cells from MOG₃₅₋₅₅-specific 2D2 mice. The levels of extracellular glutamate secreted by Th17 cells increased over time and were elevated upon TCR stimulation. Furthermore, external glutamine supply increased glutamate secretion (Figure 2A). BPTES [bis-2-(5-phenylacetamido-1,3,4-thiadiazol-2-yl)ethyl sulfide], a pharmacological blocker for the enzyme glutaminase, significantly reduced glutamate secretion following external glutamine supply (Figure 2B). Importantly, BPTES had no impact on T cell differentiation (Supplemental Figure 2A), and none of the pharmacological treatments or media affected T cell survival (Supplemental Figure 2B). In principle, intracellular glutamate can be derived either from external supplies or from de novo formation by metabolic pathways. However, we observed that mRNA levels of the enzyme glutamate oxaloacetate transaminase (*Got*) were not increased after TCR stimulation, arguing against a major role of the citric acid cycle as a metabolic glutamate source in Th17 cells (Figure 2C). A direct role of Th17 cells in neuronal damage is often doubted, given that neurons do not express the MHC class II molecules necessary for TCR-dependent recognition (30, 31). Therefore, we sought to determine the role of classical neurotoxic molecules in murine Th17 cells. Although Th1 cells produced significant amounts of granzyme B, Th17 cells expressed only very low levels of granzyme B or perforin (Figure 2D) and, surprisingly, did not express FasL (Supplemental Figure 3A). Cytokine production and transcription factor expression for differentiated Th1- and Th17-polarized cells are shown in Supplemental Figure 3, B and C. Th17 cells secreted significantly higher levels of the excitatory neurotransmitter glutamate than did undifferentiated or Th1 cells (Figure 2E), leading to the question of how Th17 cells regulate glutamate secretion and whether this secretion might have a specific role in inducing neuronal injury. We therefore assessed the expression of different pathway proteins necessary for the formation of glutamate vesicles, comparing Th1 and Th17 cells. Indeed, mRNA levels of glutaminase, vesicular H-ATPase pump, and vesicular transport proteins 1 and 2 (VGLUT1, VGLUT2) were significantly upregulated after 24 hours of stimulation in Th17 cells but not in unstimulated or stimulated Th1 cells (Figure 3A). We confirmed the upregulation of the key pathway proteins glutaminase and vesicular H-ATPase pump on Th17 cells on the protein level (Figure 3B). Therefore, we sought to determine whether Th17 cells have the same capability as neurons to transport and eventually release glutamate.

Th17 cells secrete glutamate via regulated vesicular transport. Vesicular transport relies on a number of key molecules including vesicle-associated membrane proteins (VAMPs), also termed synaptobrevins, and SNAP23, another essential component that forms the so-called soluble N-ethylmaleimide-sensitive factor attachment receptor (SNARE) complex, which is a protein complex in secretory cells. Expression of glutamate in cytotoxic T cells was previously reported, whereas the regulatory and functional roles in Th17 cells have not been addressed so far (32, 33). To unravel the potential vesicular transport of glutamate in Th17 cells via the interaction of vesicular VAMPs with target compartment membrane proteins, we first analyzed the expression of VAMP

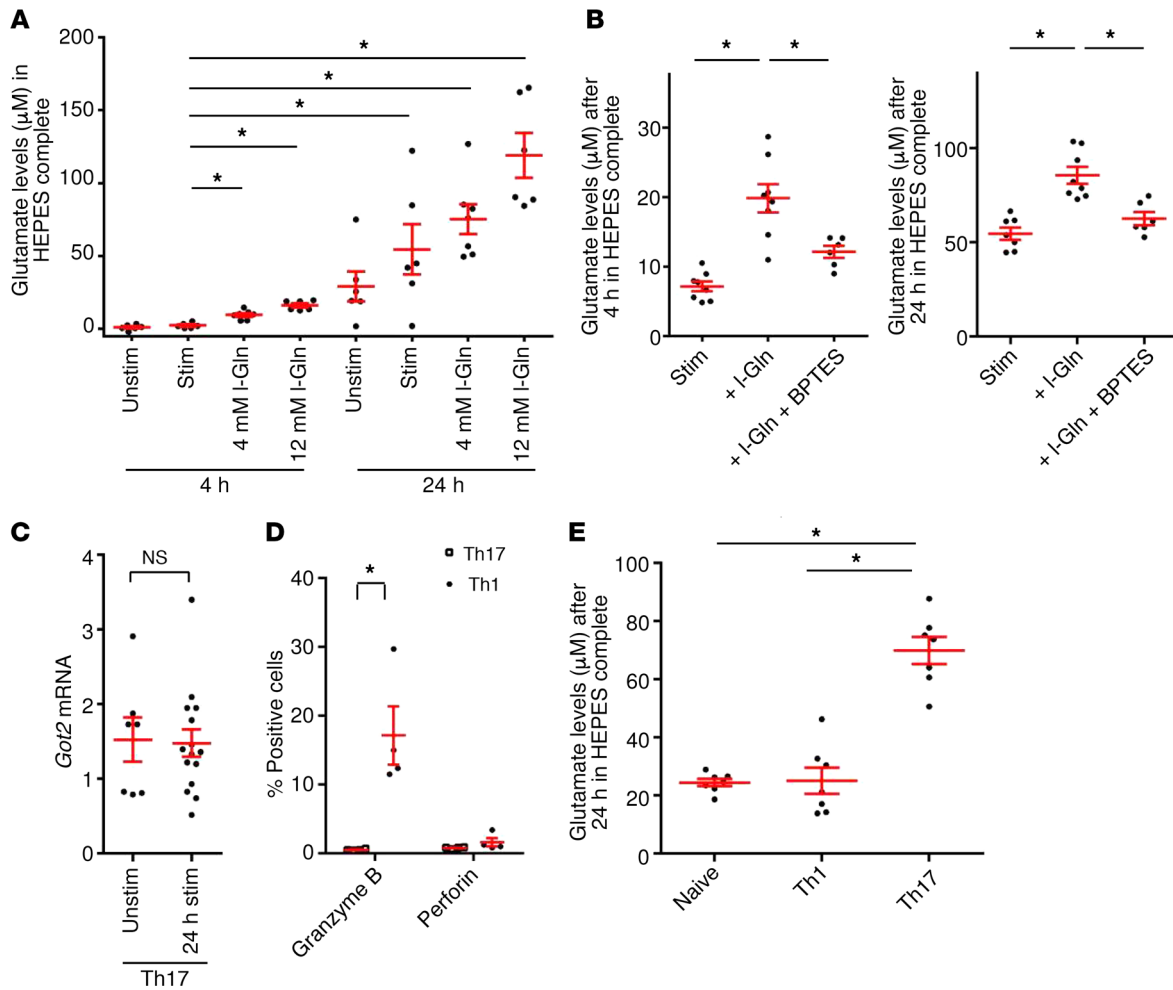


Figure 2. Th17 cells possess a vesicular glutamate release pathway. (A) Polarized murine Th17 cells from MOC₃₅₋₅-specific 2D2 mice were cultured in glutamate- and glutamine-free media or glutamine-supplemented (L-Gln) media for 4 and 24 hours, followed by measurement of glutamate levels (*n* = 6–7). (B) Glutamate levels were measured after pharmacological blocking of the enzyme glutaminase by 10 μM BPTES and external supply of 4 mM L-glutamine after 4 and 24 hours (*n* = 6–8). (C) *Got2* mRNA analysis was performed with Th17 cells compared with unstimulated Th17 cells after CD3 and CD28 stimulation (*n* = 7–15). (D) Th17 (*n* = 12) and Th1 (*n* = 5) cells were cultured for 5 days, and the levels of granzyme B and perforin were compared using flow cytometry. (E) Glutamate secretion by naive and Th1- and Th17-differentiated cells (same donors, *n* = 7) that were cultured in glutamate- and glutamine-free media for 24 hours. Data indicate the mean ± SEM. **P* < 0.05, by Mann-Whitney *U* test (C and D) or 1-way ANOVA with Tukey’s (E) or Dunnett’s (A and B) post hoc test.

proteins on Th17 cells. Indeed, we found that *Vamp2*, *Vamp3*, and *Vamp4* mRNA levels were expressed at significantly higher levels by Th17 cells than by Th1 cells (Figure 4A). We observed that SNAP23, another SNARE protein that is part of the cognate receptor complex in the target membrane, was also expressed at higher levels by Th17 cells than by Th1 cells (Figure 4A). Addition of glutamine further increased the mRNA levels of *Vamp2* and *Vamp4*, but not of *Vamp3* or *Snap23*. We confirmed the expression of SNARE complex-associated proteins by immunocytochemical and Western blot stainings of Th17-polarized CD4⁺ cells (Figure 4, B and C, and Supplemental Figure 4, A and B). To identify the role of the SNARE complex-associated proteins in vesicle glutamate release of Th17 cells, we transfected these cells with the potent tetanus neurotoxin (TeNT), which proteolytically cleaves the synaptobrevins VAMP2 and VAMP3 and thereby inhibits specific pathways of vesicular transport (34). Th17 cells transfected with a plasmid enabling TeNT expression displayed significantly decreased glutamate secretion levels compared with the non-

functional TeNT mutant (TeNT^{E234Q}) (Figure 4D). Since vesicular release of glutamate depends on Ca²⁺ and can be regulated by voltage-gated potassium channels, we assessed the effect of the specific inhibitor margatoxin (MgTX) on intracellular Ca²⁺ levels in Th17 cells after TCR stimulation. In fact, Ca²⁺-free culture conditions completely abolished glutamate secretion (Figure 4E), and blockade of K_v1.3 (KCNA3) channels with MgTX significantly reduced intracellular Ca²⁺ levels in Th17 cells after TCR stimulation (Figure 4F).

Th17 cells produce glutamate in a K_v1.3-dependent manner. We next investigated whether voltage-gated potassium channels influence vesicular release and regulate glutamate secretion by Th17 cells, as potassium channels are especially important for controlling a diverse range of T cell effector functions (35, 36). Th17 cells showed an upregulation of the voltage-gated potassium channel K_v1.3 upon TCR stimulation, and K_v1.3 currents were successfully blocked by MgTX (Figure 5A). We confirmed K_v1.3 protein expression on Th17 cells by Western blot analy-

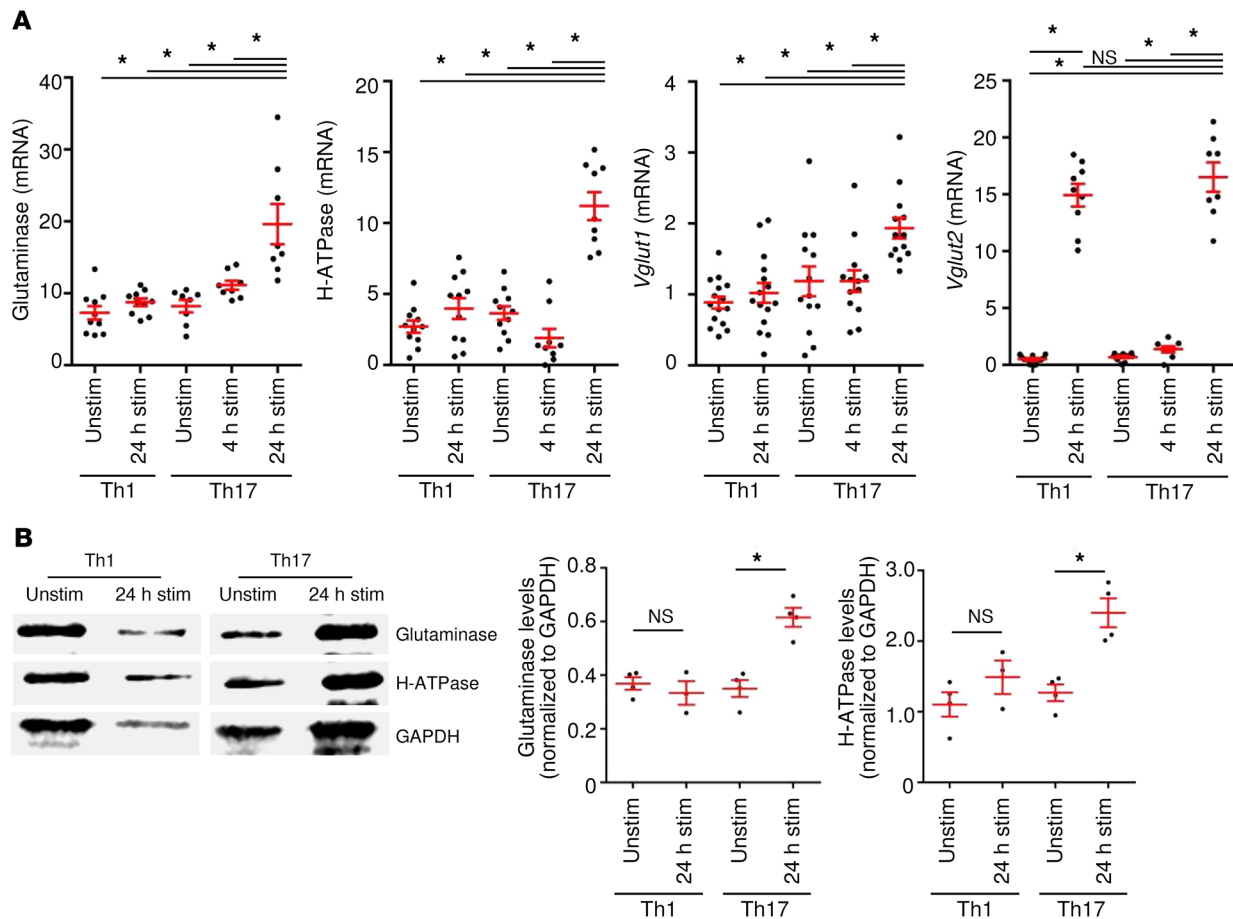


Figure 3. Upregulation of the vesicular glutamate release pathway upon stimulation. (A) mRNA analyses of the enzyme glutaminase and the vesicular transport proteins H-ATPase, *Vglut1*, and *Vglut2* were performed with unstimulated and stimulated (for 4 hours and 24 hours) Th17 cells compared with unstimulated and stimulated Th1 cells ($n = 7-15$). **(B)** Western blot analysis of unstimulated and stimulated Th1 and Th17 cells for glutaminase and H-ATPase levels. Representative blots are shown as well as quantification in relation to GAPDH levels ($n = 3-4$). Data indicate the mean \pm SEM. * $P < 0.05$, by 1-way ANOVA with Tukey's post hoc test **(A)** or Mann-Whitney U test **(B)**.

sis (Figure 5B). Th17 cells secreted significantly higher levels of glutamate after TCR stimulation, and $K_v1.3$ blockade with MgTX reversed this effect (Figure 5C). $K_v1.3$ plays an important role in the function of T effector memory cells, especially after repetitive antigen-specific stimulation, whereas blockade of $K_v1.3$ on acutely activated T cells has only minor effects (37). To investigate the role of $K_v1.3$ specifically in Th17 cells, we treated Th17-differentiated cells with MgTX. We observed that $K_v1.3$ blockade had no significant influence on T cell activation parameters such as the proliferation rate or cytokine production (Supplemental Figure 5, A and B). In contrast, we found a positive correlation between glutamate secretion and the percentage of the inflammatory cytokines IL-17 and TNF- α in Th17 cultures (Supplemental Figure 5C), indicating that Th17 cells acquire the ability to increase glutamate production during cell lineage differentiation. Additionally, $K_v1.3$ was not expressed on CNS neurons but instead on invading CD4 $^+$ T cells in EAE lesions (Supplemental Figure 5D). Although the use of 4-aminopyridine as a positive control induced neuronal glutamate release (38), $K_v1.3$ blockade did not influence neuronal glutamate secretion (Supplemental Figure 5E). Altogether, these findings point toward

a specific effect of $K_v1.3$ blockade only on T cell-mediated glutamate release during T cell–neuron interaction. To examine whether glutamate-containing vesicles can be visualized in Th17 cells, we made use of a previously published glutamate sensor (iGluSnFR) (39) that enables glutamate levels to be analyzed on the basis of GFP intensity (Figure 5D and Supplemental Figure 6). Indeed, we detected glutamate in vesicle-like structures and found that TCR stimulation led to significantly increased glutamate levels in comparison with basal levels, whereas treatment with MgTX significantly reduced both intracellular glutamate amounts and vesicle formation (Figure 5D). Importantly, MgTX had no impact on glutamate levels produced by $K_v1.3^{-/-}$ Th17 cells, underlining the specific link between $K_v1.3$ channels and glutamate secretion (Figure 5E).

K_v1.3 blockade reduces both intracellular neuronal Ca²⁺ levels and neuron damage. We previously visualized intracellular neuronal Ca²⁺ fluctuations using in vivo 2-photon laser scanning microscopy in the upper brainstem, an area prone to active inflammation in EAE (12). We induced EAE by the transfer of fluorescent myelin oligodendrocyte glycoprotein peptide-specific (MOG₃₅₋₅₅-specific) Th17-differentiated cells (2D2-RFP) into recipient mice lacking T

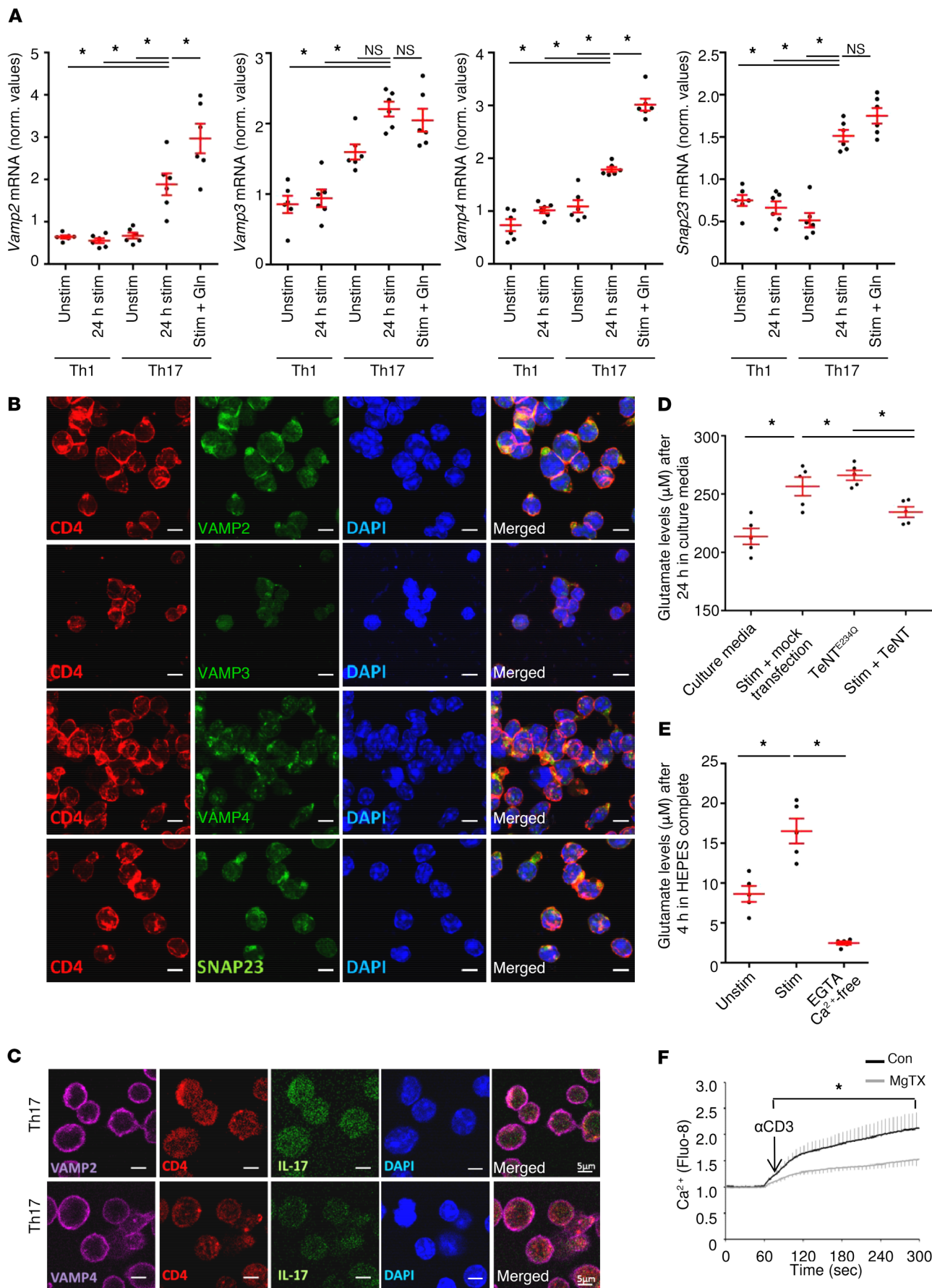


Figure 4. Th17 cells express synaptobrevins and thereby regulate the vesicular release of glutamate. (A) mRNA analysis of the SNARE complex-associated proteins was performed with unstimulated, stimulated, and stimulated plus glutamine-treated (Gln) murine Th17 cells compared with Th1 cells ($n = 6$ each). (B) Immunocytochemical staining for the synaptobrevins VAMP2, -3, -4 and SNAP23 in Th17-differentiated cells. Scale bars: 5 μm . Costaining with CD4 and DAPI was performed. (C) Immunocytochemical staining for the synaptobrevins VAMP2, VAMP4, and IL-17 in Th17-differentiated cells. Scale bars: 5 μm . Costaining with CD4 and DAPI was performed. (D) Th17 cells were transfected with TeNT and the non-functional tetanus toxin mutant (TeNT^{E234Q}). Glutamate release levels from Th17 cells per transfection were detected after 24 hours ($n = 5$ per group). (E) Th17 cells were cultured in Ca²⁺-free HEPES complete (no glutamate/no glutamine) with 2 mM EGTA, and glutamate levels were assessed after 4 hours ($n = 5$ –8 per group). (F) Ca²⁺ imaging experiments with Fluo-8 AM-loaded Th17 cells with (gray curve) or without (black curve) pretreatment with MgTX ($n = 5$ per group). αCD3 , anti-CD3; con, control. Data indicate the mean \pm SEM. * $P < 0.05$, by Mann-Whitney U test (F) or 1-way ANOVA with Tukey's (D) or Dunnett's (A and E) post hoc test.

and B lymphocytes and assessed Ca²⁺ levels via the genetically encoded Ca²⁺ indicator TN-XXL (B6.Thy1-TN-XXLxRag^{-/-}) (Figure 6A). We found that infiltrating pathogenic T cells in EAE lesions increased neuronal Ca²⁺ levels, indicating subsequent neuron damage. We assessed neuronal free Ca²⁺ levels by Förster resonance energy transfer (FRET) measurements (false color-coded representation) before and after local MgTX application. A significant reduction in neuronal Ca²⁺ elevations was observed during imaging of the EAE mice but not the healthy control animals (Figure 6, B and C, and Supplemental Videos 1 and 2). Application of Shk-186, another K_v1.3 blocker that has already entered early clinical trials in plaque psoriasis (40), produced similar effects (Figure 6D). Furthermore, coculture of primary cortical neurons with Th17 cells showed cytotoxic effects of these cells, and these effects were reversed by addition of MgTX (Figure 6, E and F). In line with previous reports (12), we observed that Th17 supernatants had no impact on neuronal cell death, underlining the importance of direct T cell–neuron contact (Figure 6F).

Th17 cells possess a β 1-integrin-controlled vesicular glutamate release pathway that is activated upon VCAM-1 engagement. As local concentrations of glutamate in a direct T cell–neuron contact could be of particular relevance, we aimed to identify whether glutamate release by Th17 cells is triggered by integrin binding on target cells. Previous studies have shown that a close physical association between K_v1.3 channels and β 1 integrins underlies their bidirectional functional coupling: integrin binding promotes K⁺ currents, and K⁺ channel function modulates integrin-mediated adherence (41, 42). Indeed, we found that Th17 cells had increased β 1-integrin expression (CD29) compared with naive and Th1 cells (Figure 7A). CD29^{hi}-expressing Th17 cells displayed higher levels of K_v1.3 and IL-17, indicating their pathogenic potential (Figure 7B). Direct activation of CD29 with an agonistic antibody as well as binding to a VCAM-1-coated surface significantly increased glutamate secretion of Th17 cells but not of Th1 cells compared with isotype controls (Figure 7C), both alone and in combination with T cell receptor stimulation. In contrast, CD29 and VCAM-1 activation had no impact on Th17 cell proliferation or cytokine production (Supplemental Figure 7, A and B). Th1 cells showed no elevated glutamate levels after activation with anti-CD29 or

anti-VCAM-1. VCAM-1 expression on neurons was significantly increased after LPS treatment and even more prominent after stimulation with splenocyte supernatant, which mimics an inflammatory environment at both the mRNA (Figure 7D) and protein (Figure 7E) levels. In inflammatory lesions from EAE animals, VCAM-1 colocalized with NeuN in neurons (Figure 7F). Whereas 38% of VCAM-1-positive neurons were localized next to invading T cells, only 1% of VCAM-1-negative neurons showed contact with T cells (Figure 7F, right). Patients with MS had increased expression of CD29 on Th17 cells compared with healthy controls (Figure 7G), and VCAM-1-positive neurons were identified in brain tissue specimens (Figure 7H; $n = 5$ patients with MS, 1 representative staining is depicted). A schematic illustration of glutamate vesicle formation and β 1-integrin/K_v1.3-mediated vesicular release by Th17 cells is shown in Figure 8.

Intrathecal blockade of either K_v1.3 or glutaminase and genetic deletion of K_v1.3 ameliorate the disease course of EAE and modulate direct cell-cell contact between T cells and neurons. To address the in vivo relevance of our findings for T cell–neuron interactions, we blocked K_v1.3 channels only in the CNS compartment in an EAE model that mimics important aspects of MS. When MgTX was injected directly into the CSF every other day for 14 days, starting on either day 7 or after disease onset (treatment started when the EAE score was >1, i.e., on day 9 or day 10) in MOG_{35–55}-specific C57BL/6 EAE, we observed a significant and reproducible reduction in the clinical score (Figure 9, A and B). In accordance with our in vitro data (Supplemental Figure 5, A and B), the differentiation of CNS-infiltrating 2D2 cells remained unchanged (Figure 9C). Importantly, we found that the degree of neuron damage was significantly smaller in MgTX-treated animals (Figure 9D).

We chose 2 approaches to assess the in vivo relevance of the newly identified neurotoxic pathway: modulation of K_v1.3 and modulation of glutaminase. First, upon in vitro differentiation, KCNA3-KO (KCNA3^{-/-}) lymphocytes displayed comparable levels of IL-17 production (Figure 10A). Passive cell transfer of KCNA3 cells induced almost no EAE symptoms in the Rag^{-/-} mice in comparison with transfer of lymphocytes from WT mice (Figure 10B). In accordance with an ameliorated disease course after K_v1.3 blockade in the CNS in vivo, the number of highly motile T cells was significantly increased, indicating fewer and shorter contacts between T cells and neurons in an inflammatory environment (Figure 10C). As an alternative approach to modulate the neurotoxic pathway described above, intrathecal administration of the glutaminase inhibitor CB-839, currently in phase I/II trials for various malignancies, also significantly ameliorated disease symptoms (Figure 10D).

Discussion

Th17 cells play a pivotal role in driving neuroinflammatory processes in patients with MS, whereas their pathological effector functions in CNS lesions are still relatively unclear (43, 44). We show here that upon activation, Th17 cells form new glutamate-containing vesicles and secrete the excitatory neurotransmitter glutamate using a vesicular release pathway mediated by β 1-integrin/K_v1.3 signaling and involving SNARE complex proteins. The SNARE complex is a protein machinery in secretory cells that is responsible

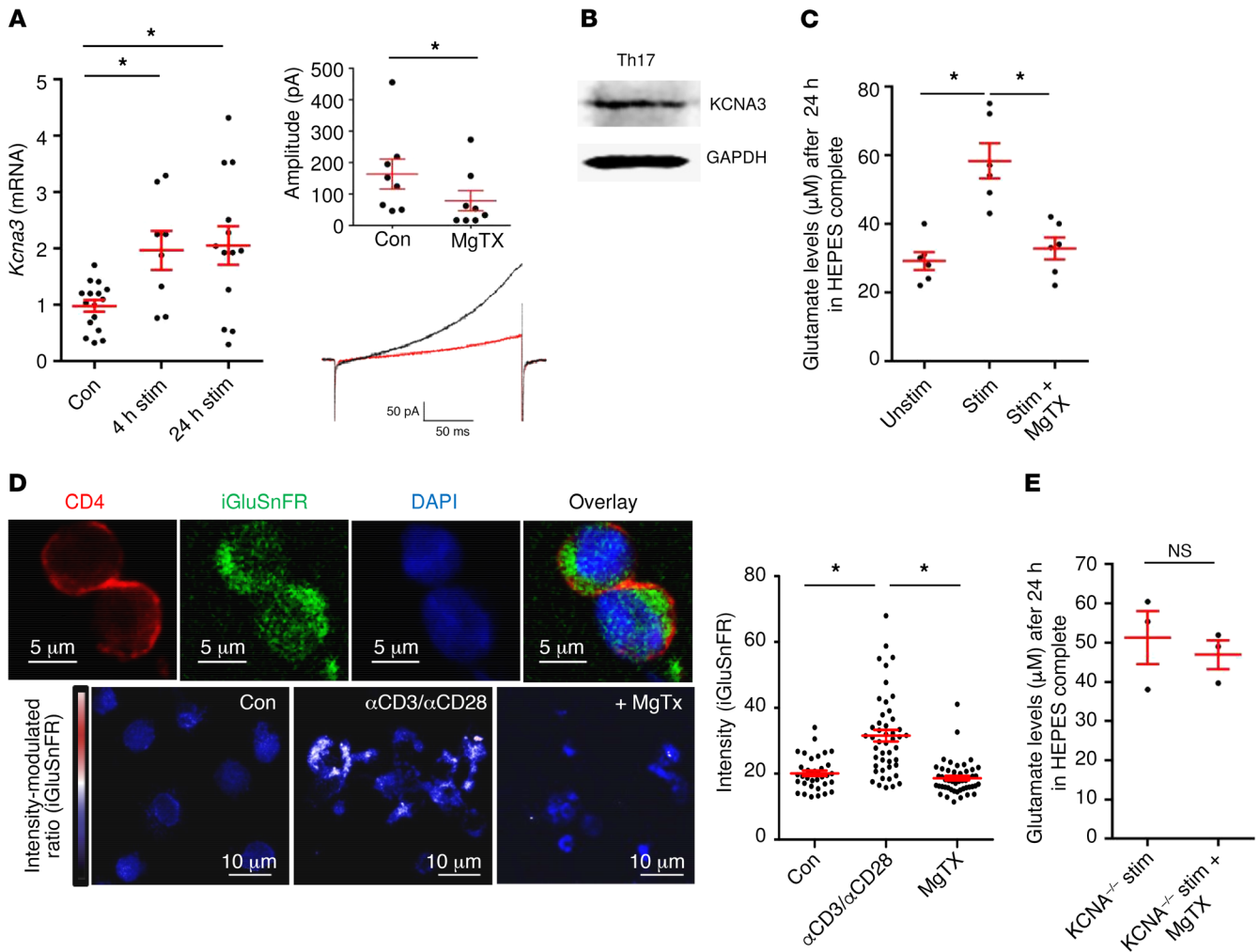


Figure 5. Th17 cells produce glutamate in a $K_v1.3$ -mediated manner. (A) *Kcna3* mRNA expression was upregulated after 4 hours and 24 hours of TCR stimulation with anti-CD3 and anti-CD28 ($n = 17$). Patch-clamp experiments were performed on Th17 cells and showed blockade of $K_v1.3$ currents after application of MgTX ($n = 9$). (B) Western blot staining for KCNA3 and GAPDH was performed in Th17 cells (1 representative example of 4 is shown). (C) Glutamate levels after 24 hours in culture media were assessed, comparing TCR-stimulated Th17 cells with or without MgTX treatment ($n = 6$ per group). (D) Th17-differentiated cells were transfected with the GFP-based glutamate sensor iGluSnFR. Staining for CD4 was also performed, and GFP intensity was analyzed with ImageJ software. Scale bars: 5 μm (top row) and 10 μm (bottom row). Data indicate the mean \pm SEM. (E) Glutamate levels were not significantly different between stimulated Th17 cells from WT and KCNA3^{-/-} mice treated with MgTX ($n = 3$ –4 per group). Data indicate the mean \pm SEM. * $P < 0.05$, by 1-way ANOVA with Dunnett’s post hoc test (A, C, and D) or Mann-Whitney U test (E).

for vesicular release, and we have discovered that Th17 cells secrete glutamate via this mechanism. SNARE complex-associated proteins have been reported in Jurkat cell lines and are hypothesized to induce TCR accumulation (33), whereas the expression, function, and regulation of these proteins in Th17 cells have not been addressed to date (33). The regulatory role of $K_v1.3$ for this pathway is intriguing and enables a functional coupling of integrin-mediated Th17–neuron adhesion in order to activate intracellular signal transduction pathways in Th17 cells. It has indeed been reported that $K_v1.3$ channels and $\beta 1$ -integrins are directly coupled, wherein the activation of integrin leads to an opening of $K_v1.3$ channels, providing the starting point for the glutamate release pathway (41). Importantly, the vesicular release pathway in Th17 cells plays a specific role in mediating neuronal damage, since VCAM-1 blockade inhibits neuronal cell death. These findings constitute a newly identified antigen presentation-independent pathway of Th17

cell-mediated neuronal damage. The upregulation of the trigger components for this glutamate release mechanism (VCAM-1 on neurons and $\beta 1$ -integrin/ $K_v1.3$ on Th17 cells) upon inflammatory conditions provides the molecular basis for T cell–neuron adhesion and thus a context-specific targeted glutamate release by Th17 cells in CNS lesions, but not in uninflamed tissue.

We also demonstrated that this mechanism is relevant in patients, since we detected (a) elevated glutamine levels in the CSF as a source for glutamate production, (b) an increase in glutaminase expression in Th17 cells, and (c) elevated glutamate secretion by Th17 cells from patients with MS. Given our findings, we argue that glutamate secretion by Th17 cells has a harmful, cell-cell contact-dependent effect on neurons upon direct adhesion and, presumably, spatially clustered T cell–neuron synapse-like formation. Although we considered the impact on neuronal Ca^{2+} elevations as a major step in a still-reversible neuronal injury sce-

nario, calculating the exact levels of local glutamate concentrations, reached locally *in vivo*, is challenging because of the complexity of the contact-site ultrastructure as well as the physical constraints of neurotransmitter diffusion. A synaptic cleft would usually be between 15–40 nm wide, leading to an estimated volume of the synaptic cleft of only 0.2 femtoliters (45). It is conceivable that glutamate concentrations in such a small T cell–neuron contact area would reach peak concentrations sufficient to trigger an elevation of neuronal calcium levels. The exact concentration is, however, difficult to directly assess as a result of the rapid decay of glutamate concentration by diffusion, reuptake, or enzymatic breakdown as well as of the density, subtype, and kinetics of post-synaptic receptors on neurons (46). Excitotoxicity for a neuron would require glutamate levels of 5 μM or higher.

Importantly, VCAM-1 upregulation on neurons themselves can be seen as a neuronal signaling receptor, increasing the likelihood of Th17 cell–neuron interaction that would lead to local release of excessive amounts of glutamate molecules. Th17 cells might therefore be able to recognize specifically inflamed neurons and engage in potentially harmful and stable T cell–neuron contact formations. In addition to glutamate-mediated intracellular calcium increases, other pathways such as those for oxidative stress and mitochondrial dysfunction will influence the extent and outcome of neuron injury. The identification of local, targeted glutamate release adds an important piece of information necessary to unravel the complex interplay of immune and neuronal cells within inflammatory CNS lesions.

Using *in vivo* 2-photon imaging, we were able to demonstrate that by reducing Th17 cell-derived glutamate excitotoxicity, $K_v1.3$ inhibitors significantly reversed already elevated Ca^{2+} levels in neurons, indicating possible therapeutic potential by directly reducing T cell-mediated neuron injury. $K_v1.3$ is not expressed on CNS neurons. However, to specifically focus on CNS parenchymal effects in neuroinflammation, we administered $K_v1.3$ blockers intrathecally into the CSF. Most important, induction of EAE via adoptive transfer of Th17 cells from $Kv1.3^{-/-}$ mice resulted in an even more pronounced phenotype. The importance of the voltage-gated potassium channel $K_v1.3$ for autoreactive effector memory T cells has been recognized (35, 47–49), and the $K_v1.3$ blocker Shk-186 has been tested in 2 phase I trials involving healthy volunteers and patients with psoriasis (NCT02446340 and NCT02435342; www.clinicaltrials.gov). Our findings point to a fundamental role of Th17 $K_v1.3$ channels in inflammatory lesions in the CNS. Blocking these channels directly targeted a cytotoxic effector pathway under the control of a $\beta 1$ -integrin/ $K_v1.3$ signaling pathway.

Finally, we identified targeted glutamate excitotoxicity as a Th17 cell effector pathway in neuroinflammation, directed to neurons under the control of a VCAM-1/ $\beta 1$ -integrin/ $K_v1.3$ signaling axis. These studies lay the groundwork for further investigations of glutamate-producing and -sensing cells in the inflammatory microenvironment of MS lesions and the development of therapeutic treatments for patients with MS.

Methods

Passive EAE. Mice were bred under specific pathogen-free conditions and kept in-house for experiments in individually ventilated cages. Neuronal Ca^{2+} indicator mice (B6.Thy1-TN-XXLxRag2 $\gamma\text{C}^{-/-}$ mice) were

originally obtained from Oliver Griesbeck (Department of Systems and Computational Neurobiology, Max Planck Institute of Neurobiology, Martinsried, Germany). B6.2D2.RFP mice, in which all CD4^+ T cells are MOG_{35–55} specific, were obtained by crossbreeding B6.acRFP and B6.2D2 mice. Passive EAE in B6.Thy1-TN-XXLxRag2 $\gamma\text{C}^{-/-}$ mice was induced by *i.v.* transfer of 1×10^7 Th17-differentiated B6.RFPx2D2 cells.

Female C57Bl/6 J mice (Janvier Labs) and $\text{KCNA3}^{-/-}$ mice (originally obtained from The Jackson Laboratory) were immunized *s.c.* with a Hooke Kit EK-2110 (MOG_{35–55} peptide) according to the manufacturer's instructions. Ten days later, lymph nodes were isolated and stimulated with MOG_{35–55} (20 $\mu\text{g}/\text{mL}$) in the presence of TGF- β (4 ng/mL), IL-6 (20 ng/mL), IL-23 (20 ng/mL), anti-IFN- γ (10 $\mu\text{g}/\text{mL}$), and anti-IL-4 (10 $\mu\text{g}/\text{mL}$) for 4 days in a T75 flask. Lymph nodes were collected and sorted for CD4^+ cells and then injected *i.v.* (6.5×10^6 cells/mouse) into the mice. The mice were scored daily. Clinical signs of EAE were translated into the following clinical scores: 0 = no detectable signs of EAE; 1 = complete tail paralysis; 2 = partial hind limb paralysis; 3 = complete bilateral hind limb paralysis; 4 = total paralysis of forelimbs and hind limbs; 5 = death.

Active EAE. Six- to eight-week-old female C57Bl/6 J mice were *s.c.* immunized with the Hooke Kit EK 2110 (MOG_{35–55} peptide) according to the manufacturer's instructions. Treatment with MgTX (1.3 ng/mouse) (Tocris) or vehicle (PBS) was performed 7 times (every other day starting either preclinically from day 7 after immunization or therapeutically, when mice reached a score of 1 [-day 12]) by lumbar intrathecal injection (50). In another set of experiments, mice were treated intrathecally with the glutaminase inhibitor CB-389 (5 μM in 5 μL). Clinical signs of EAE were translated into clinical scores as described above.

Murine cell culture. Naive $\text{CD4}^+\text{CD62L}^+$ cells from spleens and lymph nodes of B6.2D2, B6.RFP.2D2, and $\text{KCNA3}^{-/-}$ mice (6 to 10 weeks of age) were isolated and MACS sorted, with a purity of greater than 95% of total cells. Murine Th17 cell differentiation was achieved by the addition of 2 $\mu\text{g}/\text{mL}$ anti-CD3, 3 ng/mL TGF- β , 20 ng/mL mIL-6 , 20 ng/mL IL-23, 10 $\mu\text{g}/\text{mL}$ anti-IL-4, and 10 $\mu\text{g}/\text{mL}$ anti-IFN- γ . Murine Th1 cell differentiation was achieved by the addition of 2 $\mu\text{g}/\text{mL}$ anti-CD3, 50 ng/mL IL-12, 25 ng/mL IL-18, and 10 $\mu\text{g}/\text{mL}$ anti-IL-4.

Irradiated antigen-presenting cells (APCs) were used for initial stimulation of the Th17 lymphocytes at a 1:10 ratio and for the Th1 lymphocytes at a 1:5 ratio. Cells were kept in cell culture medium and then split with 50 U/mL IL-2 and 10 ng/mL IL-23. After 7 days in culture, the cells were restimulated with fresh APCs. T cells were generally taken for transfer on day 10 and showed IL-17 production of greater than 30%. Cells that produced more than 30% of IL-17 were used for *in vitro* assays. Cytokine production was assessed using either intracellular cytokine staining following standard protocols (CD4-PeCy7, clone RM4-5, BD Biosciences; IL-17A-AF647, clone 17B7, Affimetrix; IFN- γ -Horizon, clone XMG1.2, BD Bioscience; TNF- α -AF700, clone MP6-XT22BD, eBioscience; FoxP3-PeCy7, clone FJK-16s, Invitrogen, Thermo Fisher Scientific; Tbet-PE, clone 4B10, eBioscience; and CD4-V450, clone RM4-5, BD Biosciences) with LIVE/DEAD Fixable Dead Cell Stain AF700 (Thermo Fisher Scientific), or by cytokine bead array (LEGENDplex, BioLegend). Additional flow cytometric analysis was performed by labeling with the following antibodies: CD29-PE (clone HM $\beta 1$ -1, BD Biosciences), granzyme B-Pacific Blue (clone GB11, BioLegend), and perforin-APC (clone eBioOMAK-D, Thermo Fisher Scientific). When comparing Th1 and Th17 cells, both cultures were obtained from the same mice.

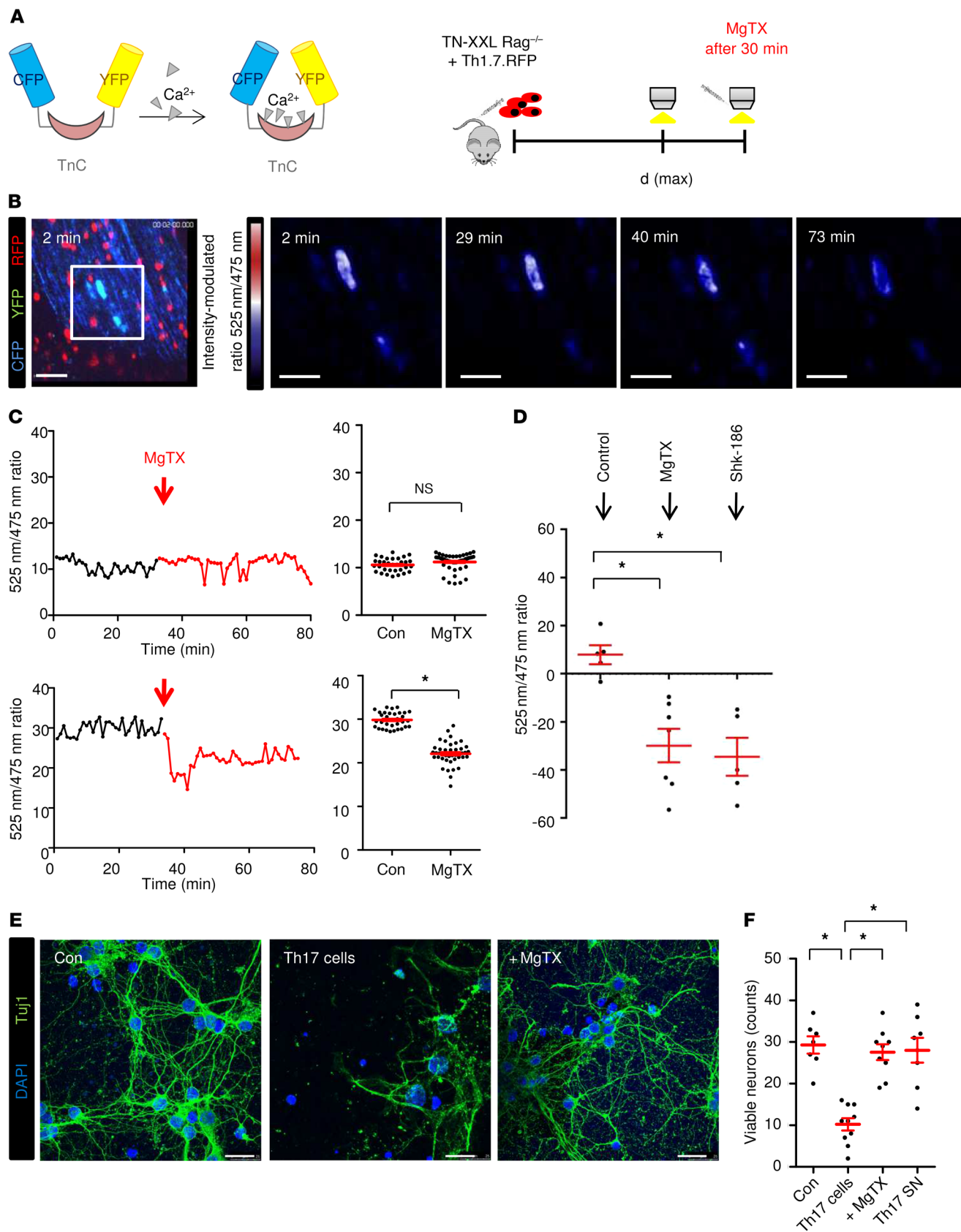


Figure 6. Immune-mediated neuronal Ca^{2+} elevations and neuronal damage can be significantly diminished by blockade of $\text{K}_v1.3$ channels in vivo. (A) EAE was induced in B6.Thy1-TN-XXLxRag2 $\gamma\text{C}^{-/-}$ mice (TN-XXL Rag $^{-/-}$) via the passive transfer of CD4^+ cells from B6.2D2.RFP.Th17 cells (Th17.RFP). At the peak of disease [d(max)], Ca^{2+} levels were imaged in vivo with intravital 2-photon imaging (TnC refers to troponin, a Ca^{2+} binding protein within the TN-XXL construct, comprising the genetically encoded calcium indicator). (B) Neuronal free Ca^{2+} levels were assessed by FRET measurements (false color-coded representation) before and after MgTX application (5 μM) in healthy control and EAE mice. Scale bars: 60 μm . B6.2D2.RFP.Th17 cells are shown in red. Ca^{2+} fluctuations were assessed by the 525 nm/475 nm ratio ($\Delta\text{R}/\text{R}$). Scale bars: 30 μm . (C) Quantification of the full field 525 nm/475 nm ratio ($\Delta\text{R}/\text{R}$) in healthy control mice (upper graphs, $n = 32$ control neurons, $n = 48$ MgTX neurons) and EAE mice (lower graphs, $n = 33$ control neurons, $n = 42$ MgTX neurons). Data were included from 7 control mice and 12 MgTX-treated mice (EAE score >2 from 2 independent experiments). (D) Changes in whole-field analysis of ratio channel intensities after application of 2 different $\text{K}_v1.3$ blockers in vivo: MgTX ($n = 7$) and Shk-186 ($n = 5$). (E) Neuronal cortical cultures were incubated with Th17 cells for 12 hours with or without MgTX. Neurons were stained with Tuj1 and DAPI. Scale bars: 25 μm . (F) Quantification of viable neurons after application of Th17 cells with or without MgTX ($n = 7$ –10) and T cell supernatant for 12 hours ($n = 7$). The y axis represents viable counts per $165 \times 165 \mu\text{m}$. Data represent the mean \pm SEM. * $P < 0.05$, by unpaired Student's t test (C) or 1-way ANOVA with Tukey's post hoc test (D and F).

Cortical neuronal cell culture. For neuronal cultures, E17 embryos from C57BL/6 mice were taken, and brains were removed from the skull. The brains were prepared in ice-cold HBSS. The olfactory bulbs and the meninges were removed from the cortex. The hippocampus was stripped from the cortex, and all cortices were collected in ice-cold HBSS. Cortices from up to 3 animals were pooled into 1 Falcon flask. The tissue was washed once with ice-cold HBSS and digested in HBSS with 1% DNase and 0.5% trypsin for 20 minutes at 37°C. For homogenization, tissue was sucked through 2 small glass pipettes and finally poured over a 70- μm cell sieve. Cells (500,000–750,000 cells) were seeded in each well of the 6-well plate in plating medium. After 3 hours, cells were washed with neurobasal medium. The cultures were washed every 2 to 3 days.

Neuronal cultures were inflamed between day 7 and day 8, and cultures were harvested 24 hours later, between day 8 and day 9. Cells were harvested with 3% trypsin for 5 minutes at 37°C, washed from the plates, and collected on ice. The cells were centrifuged for 5 minutes at 550 g at 4°C and washed once with ice-cold PBS. Pellets for mRNA and Western blot analysis were frozen at -80°C .

Human cell cultures. Samples of total blood or CSF from 63 patients who met the revised McDonald criteria for MS (51) were included in this study (Supplemental Tables 1–3). All patients who donated blood had not received previous treatment or immunosuppressive agents for at least 6 months before the time of analysis and were clinically stable. CSF was drawn at the time of the first diagnosis (noninflammatory neurological diseases, $n = 14$); relapsing-remitting multiple sclerosis (RRMS) (see Supplemental Table 1). PBMCs from 37 healthy individuals served as controls.

PBMCs were isolated and sorted for CD4^+ cells (see Supplemental Tables 2 and 3). For human Th17 cell differentiation, $\text{CD4}^+\text{CD45RO}^+$ cells were isolated and cultured for 5 days with IL-23 (10 ng/mL), anti-IL-4 (5 $\mu\text{g}/\text{mL}$), anti-IFN- γ (5 $\mu\text{g}/\text{mL}$), OKT-3 (2.5 $\mu\text{g}/\text{mL}$), and anti-CD28 (2 $\mu\text{g}/\text{mL}$). IL-23 was added again on day 3. For human Th1 cell differentiation, cells were cultured for 5 days with IL-12 (10 ng/

mL), anti-IL-4 (5 $\mu\text{g}/\text{mL}$), OKT-3 (2.5 $\mu\text{g}/\text{mL}$), and anti-CD28 (2 $\mu\text{g}/\text{mL}$). Th1 or Th17 cells were stimulated with PMA (1:1000) and ionomycin (1:1000) for 24 hours in X-Vivo Media (Lonza) supplemented with 1% glutamine and 1% penicillin-streptavidin. Brefeldin A (1:1000) was added to stop cytokine secretion. Flow cytometric analysis was performed using CD4-FITC (clone M-T466, Miltenyi Biotec), CD3-AF700 (clone UCHT1, BD Biosciences), IL-17-APC (clone eBio-64DEC17, Thermo Fisher Scientific), TNF- α -PeCy7 (clone Mab11, BD Biosciences), IFN- γ -V450 (clone B27, BD Biosciences), and CD29-PE (clone TS2/16, BioLegend). CSF samples were thawed and directly used for analysis (see Supplemental Table 1). When comparing human Th1 and Th17 cells, both cultures were obtained from the same donors.

Determination of supernatant glutamate levels. Supernatant glutamate levels were determined after in vitro stimulation with anti-CD3 (3 $\mu\text{g}/\mu\text{L}$) and anti-CD28 (2.5 $\mu\text{g}/\mu\text{L}$) of B6.WT or B6.2D2 $\text{CD4}^+\text{IL-17}^+$ T cells using a commercially available enzymatic determination kit (Glutamate Assay Kit, MAK004, MilliporeSigma) following the manufacturer's instructions. Glutamate levels were also detected in the supernatant of B6.2D2 $\text{CD4}^+\text{IL-17}^+$ T cells that were activated with 2 $\mu\text{g}/\text{mL}$ of the CD29 agonistic antibody (clone KMI6, Invitrogen, Thermo Fisher Scientific) and after 10 $\mu\text{g}/\text{mL}$ recombinant mouse VCAM-1 Fc chimera protein stimulation (R&D Systems). Background glutamate levels were determined in the absence of cells and subtracted from those obtained during incubation and stimulation of the cells. Experimental values were interpolated in Excel within a standard curve of 0, 2, 4, 6, 8, and 10 nmol/well. All blockers were incubated for the same durations and diluted in the same media. For estimation of glutamate secretion kinetics, cells were cultured in glutamate-free HEPES complete containing 120 mM NaCl, 2.5 mM KCl, 1.25 mM NaH_2PO_4 , 30 mM HEPES, 2 mM MgSO_4 , 10 mM glucose, and 2.64 mM CaCl_2 (pH 7.2).

Determination of CSF glutamine levels. Glutamine levels in human CSF samples were determined using the Glutamine Detection Assay Kit (ab197011, Abcam) following the manufacturer's instructions. The assay is based on the hydrolysis of glutamine to glutamate, which produces a stable signal that is directly proportional to the amount of glutamine in the sample. Experimental values were interpolated in Excel within a standard curve of 0, 2, 4, 6, 8, and 10 nmol/well.

Western blot analysis. Cortex neurons were harvested using trypsin-EDTA (MilliporeSigma) diluted 1:3 in Dulbecco's PBS (DBPS) (MilliporeSigma), washed twice with DPBS, and centrifuged at 550 g for 5 minutes. The cell pellet was then frozen at -80°C until cell lysis. Th1 and Th17 cells were washed with DBPS and treated in a similar manner. Then, protein samples were lysed using RIPA buffer (MilliporeSigma) that included a protease inhibitor cocktail (Roche). The total protein concentration was determined by Bradford assay using a BSA standard. After a 5-minute incubation step with Bradford Ultra (Expedeon), the absorption was detected at 595 nm in the Tecan Reader (Tecan Infinite M200 PRO) using Tecan i-control 1.11 software. The concentration was calculated using a regression curve with a coefficient of determination of R greater than 0.93. Total protein (14 μg) was separated by SDS-PAGE (12% acrylamide). The proteins were transferred onto a 0.45- μm nitrocellulose membrane (Bio-Rad) using the wet blot method. Unspecific binding sites were blocked with 5% milk powder diluted in TBS containing 0.1% Tween (TBST) for 1 hour at room temperature. The membranes were incubated with anti- β -actin (MP Biomedicals, 1:10,000), anti-VCAM-1 (Abcam, 1:10,000),

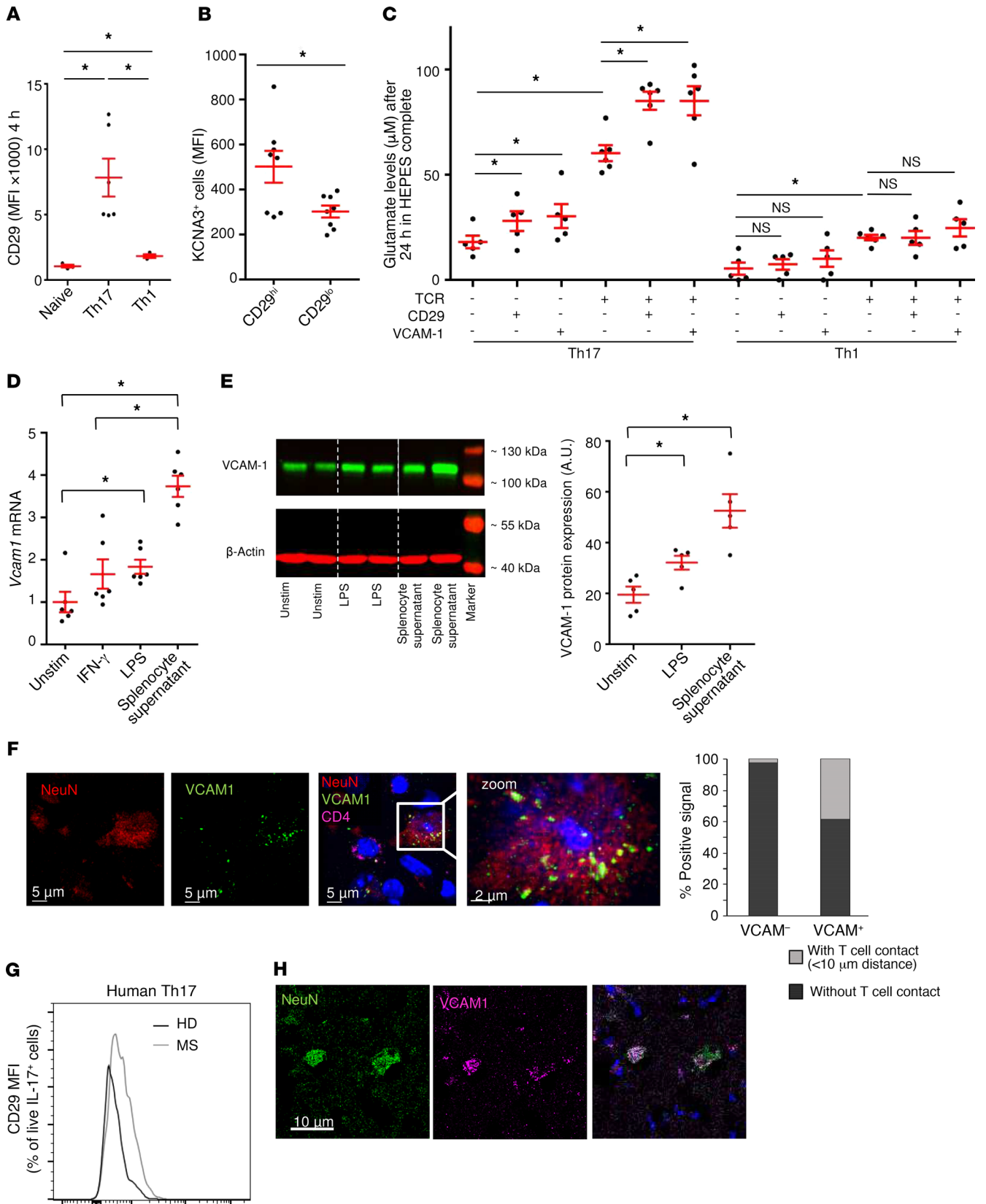


Figure 7. $K_v1.3$ -mediated glutamate release is enhanced by activation of $\beta 1$ -integrin (CD29) and upon VCAM-1 binding. (A) Naive, Th17, and Th1 cells were stimulated for 4 hours and stained for CD29. Mean fluorescence intensity (MFI) is shown ($n = 3-6$). (B) Flow cytometric staining for KCNA3 expression ($n = 6$) and IL-7 production ($n = 6$) was performed on Th17 cells, comparing CD29^{hi}- and CD29^{lo}-expressing cell populations. (C) Glutamate levels in unstimulated or TCR-stimulated Th1 and Th17 cells with additional CD29 stimulation or VCAM-1 coating ($n = 10-12$ per group), 24 hours after culturing in HEPES complete. (D) *Vcam1* mRNA expression levels in cortical neurons that were unstimulated, treated with IFN- γ , or stimulated with LPS, and after application of splenocyte supernatant ($n = 5-9$). (E) VCAM-1 protein analysis and quantification of cortical neurons with or without LPS stimulation or splenocyte supernatant addition. Western blot analysis showed protein levels in kDa ($n = 3-4$). (F) Immunohistochemical staining for VCAM-1 in infiltrated EAE lesions. Scale bars: 6 μ m and 2 μ m (zoom, enlarged inset). $n = 8$ animals from 2 independent EAE experiments; cells were isolated at the maximum disease stage. Costaining for NeuN and CD4 was performed. Graph shows quantification of VCAM-1-positive and -negative cells with or without T cell contact. (G) CD29 extracellular staining for CD29 in human MS Th17 cells ($n = 6$) compared with cells from healthy donors ($n = 5$). (H) VCAM-1-positive neurons were identified in brain tissue specimens from patients with MS ($n = 5$ patients with MS; 1 representative staining is shown). Scale bar: 10 μ m. Data indicate the mean \pm SEM. * $P < 0.05$, by unpaired Student's *t* test (B), 1-way ANOVA with Tukey's (A, C, and D) or Dunnett's (E) post hoc test.

anti-glutaminase (Abcam, 1:5,000), anti-H-ATPase (Bioss Antibodies, 1:1000), anti-KCNA3 (Alomone Labs, 1:500), anti-VAMP4 (Synaptic Systems, 1:1,000), or anti-GAPDH (Abcam, 1:10,000), washed, and then incubated with secondary antibodies conjugated with infrared fluorescent dyes (LI-COR Biotechnology; 1:20,000). Protein bands were detected using the LI-COR Odyssey imaging device (LI-COR Biotechnology). Quantification was done using Image Studio Lite software (LI-COR Biosciences).

Quantitative real-time PCR. For analysis of mRNA expression of *Kcna3*, glutaminase, *Got2*, H-ATPase, the vesicular glutamate transporters *Vglut1* and *Vglut2*, as well as *Vamp1*, *Vamp2*, *Vamp3*, *Vamp4*, and *Snap23*, RNA was isolated using the RNeasy Mini Kit (QIAGEN) according to the manufacturer's protocol. The quality and integrity of total RNA preparation were confirmed using a NanoDrop 2000c Spectrophotometer (Thermo Fisher Scientific). cDNA synthesis was performed by reverse transcription of total RNA using the SuperScript III First Strand Synthesis System and random hexamer primers (all from Invitrogen, Thermo Fisher Scientific) according to the manufacturer's instructions. Amplification primers for real-time PCR analysis were designed using Beacon Designer 8 Software (PREMIER Biosoft International) according to the manufacturer's guidelines and subsequently tested for amplification efficiency and specificity. The sequences for the primers are listed in Supplemental Table 4. Real-time PCR was performed using iQ SYBR Green Supermix (Bio-Rad) in the CFX Connect Real Time Detection System (Bio-Rad). Relative changes in gene expression were determined using the Ct method (52) with *Actb* as the reference gene.

Electrophysiological measurements. Patch-clamp experiments were performed on Th17 cells initially incubated on poly-L-lysine (PLL) coverslips (minimum 30 minutes). Whole-cell configurations from Th17 cells were recorded by eliciting a 200-ms depolarizing voltage ramp from -100 mV to +30 mV every 20 seconds. $K_v1.3$ currents were assessed before and after application of MgTX. $K_v1.3$ currents were recorded in artificial CSF solution containing 125 mM NaCl, 2.5 mM

KCl, 1.25 mM NaH_2PO_4 , 30 mM HEPES, 2 mM MgSO_4 , 2 mM CaCl_2 , 10 mM glucose (pH 7.35 with NaOH; 305 mOsm/kg) constantly oxygenated with 5% CO_2 and 95% O_2 . In all experiments, a GB200F-10 microelectrode (6-11 MOhm) was used. Microelectrodes were filled with an intracellular solution containing 88 mM K-gluconate, 20 mM K3-citrate, 15 mM phosphocreatine, 10 mM NaCl, 10 mM HEPES, 1 mM MgCl_2 , 0.5 mM CaCl_2 , 3 mM 1,2-bis(2-aminophenoxy)ethane-*N,N,N',N'*-tetraacetic acid (BAPTA), 3 mM Mg-ATP, and 0.5 mM Na3-GTP (pH 7.25 with KOH; 295 mOsm/kg). Whole-cell $K_v1.3$ conductances were calculated from the peak current amplitudes at +30 mV. Cell capacitance, a direct measure of cell surface area, was constantly monitored during the recording.

Fluo-8 Ca^{2+} measurements. To measure intracellular Ca^{2+} levels, 1×10^6 Th17 cells were loaded with the synthetic Ca^{2+} indicator Fluo-8 AM (Santa Cruz Biotechnology) for 15 minutes at 37°C in HEPES Complete (for the ingredients, see above). Anti-CD3 (10 μ g/mL) and MgTX (10 μ M) were added for another 15 minutes at 37°C. Fluorescence imaging was performed using a Tecan Infinite 200 PRO microplate reader including an injector function, which was used for real-time anti-CD3 cross-linking via goat anti-Armenian hamster IgG (H+L) (Jackson ImmunoResearch). Fluorescence signals with an excitation wavelength of 490 nm and an emission wavelength of 525 nm were assessed.

Proliferation assay. Th17 cells were cultured for 10 days as described above, and plates were cultured in 5% CO_2 for 72 hours at 37°C; 18.5 kBq of [3H]-thymidine was added for the final 72 hours of cultivation before harvesting. A CFSE proliferation assay was performed by incubating Th17-differentiated cells in mouse medium at 37°C for 30 minutes, and then cells were washed twice with prewarmed RPMI plus 1% HEPES (RH) and then dissolved in CFSE in prewarmed RH at a concentration of 2.5 μ M. After quenching the stained cells with cold mouse medium, cells were incubated for at least 72 hours and evaluated by flow cytometry.

Intravital 2-photon imaging. Passive EAE was induced as described above. The operation procedures and 2-photon laser scanning microscopy were performed as described previously (2, 12, 53, 54). B6.Thy1-TN-XXLxRag2 γ c^{-/-} mice with an EAE disease score of 2.0-3.0 were anesthetized and continuously respired using 1.5% isoflurane (Abbott) in oxygen/nitrous oxide (1:2) with a face mask. For imaging, the animal was transferred onto a custom-built microscopy table and the head inclined to allow access to regions deeper in the brainstem, an area involved in CNS autoimmunity. The dura mater was removed, and a sterile agarose patch (0.5% in 0.9% NaCl solution) was installed and used to capture the PBS bath that was continuously exchanged by a peristaltic pump. During surgery and imaging, the animal's body temperature was maintained at 34°C-37°C, and vital signs were monitored. We applied dual near-infrared and infrared (IR) excitation of the live brainstem at 850 nm by a tunable Ti:Sa laser (Mai Tai HP, Spectra Physics) and at 1110 nm by an optical parametric oscillator (OPO) (APE) pumped by the Ti:Sa laser. Volumes of 300 \times 300 \times 72 μ m were acquired using an Olympus XLUMPlanFI \times 20/0.95 W objective on a TriMScope I from LaVision Biotec and exported as TIFFs for 3D analysis, with a temporal resolution of 1 frame/minute.

Immune cells (red fluorescent protein [RFP]) infiltrate the upper brainstem region and show close proximity with somata and axons (TN-XXL = yellow fluorescent protein [YFP], cyan fluorescent protein [CFP]). TN-XXL is expressed under the neuron-specific Thy1

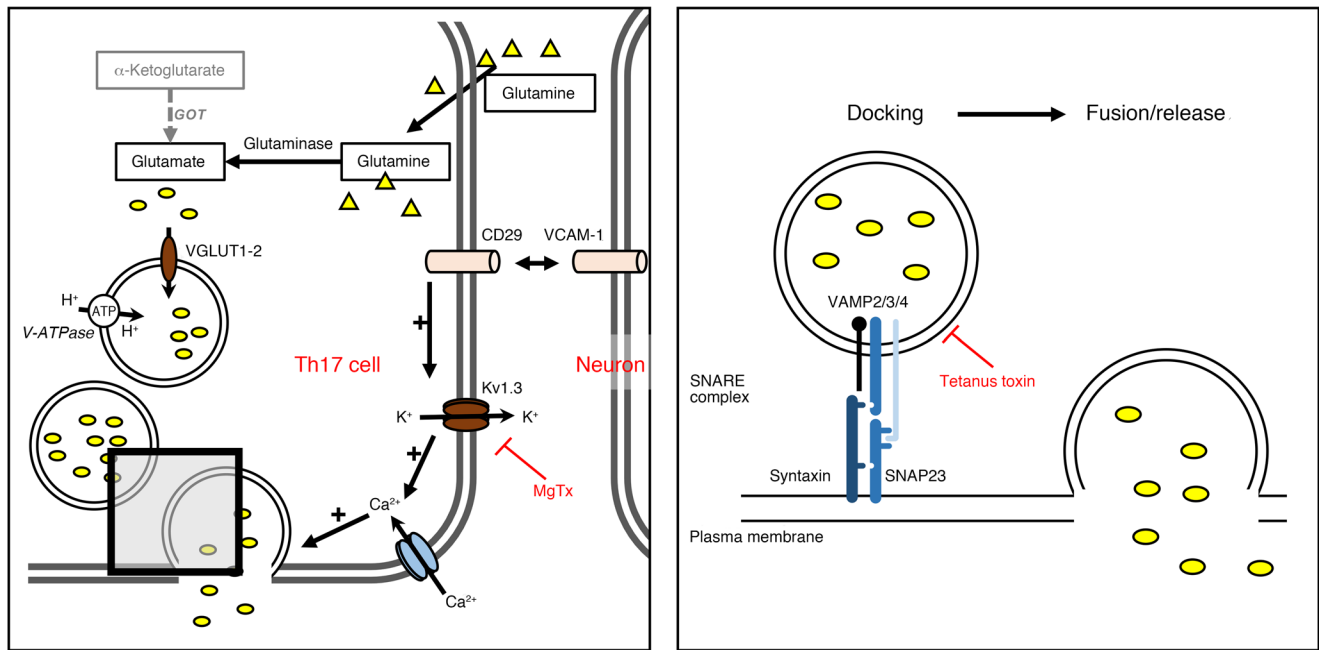


Figure 8. Schematic illustration of Ca^{2+} -dependent vesicular glutamate release from Th17 cells, which is counterbalanced by blockade of $\text{K}_v1.3$ channels.

The schematic illustrates glutamate vesicle formation and release with its main players: external glutamine, glutaminase, the vesicular proton ATPase pump, the vesicular transport proteins VGLUT1 and VGLUT2, and the SNARE complex, as well as the initiation of an integrin/ $\text{K}_v1.3$ -mediated release pathway.

promotor and allows the measurement of relative Ca^{2+} changes by computing the ratio of YFP to CFP fluorescence that shifts via a FRET (55, 56). For ratiometric analyses, acquired XYZ-stacks of CFP and YFP channels were exported as TIFF files and post-processed by Volocity software (Improvision). For visualization of the mean YFP/CFP ratio in the neurons, an intensity modulated ratio (IMR) channel was generated and exported as a TIFF file and false color coded (unionjack, ImageJ, NIH). For quantification of the time-dependent intraneuronal Ca^{2+} per volume of the neuronal structures, clearly discernable neurons were identified in the CFP channels by object recognition in Volocity and IMR, and volume data for all CFP structures and time points were further processed and analyzed using Origin software (OriginLab Software).

MgTx (5 μM) was puffed locally during imaging of the EAE mice. In an additional set of experiments, healthy TN-XXL Rag^{-/-} mice were imaged in the same manner. T cell tracks were created using the tracking tool in Imaris software (Bitplane, version 8.1.2). On average, 20–100 T cells were analyzed per field of view in 1 in vivo experiment. For T cell motility analysis 30 cells reflecting the mean velocities per video were included for further analysis.

Immunohistochemistry. Neuronal cortical cultures (370,000 cells/well) were incubated with 100,000 Th17 cells per well for 12 hours with or without 1 μM MgTx for 24 hours. In another set of experiments, supernatant from stimulated Th17 cells was added instead. Immunohistochemical analysis was performed with these cocultures of neurons and with tissue from EAE brainstems of B6.2D2 mice. $\text{K}_v1.3$ channels were stained using mouse anti- $\text{K}_v1.3$ -AF647 (BD Biosciences) and anti-mouse AF647 (Invitrogen, Thermo Fisher Scientific). Anti-mouse CD4-AF647 was used to stain for CD4 (BD Biosciences). Neurons were stained for Tuj-1 (TubIII, Covance), NeuN (MilliporeSigma), and VCAM-1 (clone EPR5047, Abcam). Th17 cells were stained for CD4-AF647 (BD

Biosciences), VAMP2, -3, and -4 (Synaptic Systems), SNAP23 (Synaptic Systems), and IL-17-FITC (BD Biosciences). Cell nuclei were stained with DAPI (Invitrogen, Thermo Fisher Scientific).

Human autopsy and biopsy materials from 5 subjects with MS were received from the UK Multiple Sclerosis Tissue Bank (Division of Neuroscience and Mental Health, London, United Kingdom). The lesions fulfilled the morphologic criteria of an inflammatory demyelinating process consistent with MS when stained with H&E, LFB, and periodic acid-Schiff (PAS) or with myelin stain and Bielschowsky's silver impregnation for axons. We classified lesions according to their demyelination status and included 1 early active, 1 late active, and 3 inactive lesions. Staining was performed on 10- μm coronal sections. For double labeling, the slices were fixed in 4% paraformaldehyde (PFA) and incubated in blocking solution (5% BSA [PAA], 1% normal goat serum [paa], and 0.2% Triton X-100) (MilliporeSigma). Afterwards, the coronal slices were incubated with antibodies against VCAM-1 (1G11B1, Acris) and NeuN (MilliporeSigma) and the respective secondary antibodies (Alexa Fluor 488 and 647, Abcam). Images were acquired with a Leica TCS-SP8 confocal laser scanning microscope.

Cryosections of EAE mouse brains were stained for SMI312 (Abcam) and quantified in a blinded manner. Images were acquired with an Olympus microscope equipped with a cellSens camera and analyzed with ImageJ software (NIH).

Immunoelectron microscopy. Immunoelectron microscopy was performed according to previously described procedures (57). Briefly, unstimulated or stimulated human Th17 cells were fixed for 3 hours in 0.1% glutaraldehyde and 4% PFA. After a stepwise dehydration in ethanol, cells were embedded in LR White (Science Services), cut into ultrathin 60-nm sections with a Leica Ultracut S, and collected on Formvar-coated (Roth-coated) nickel grids

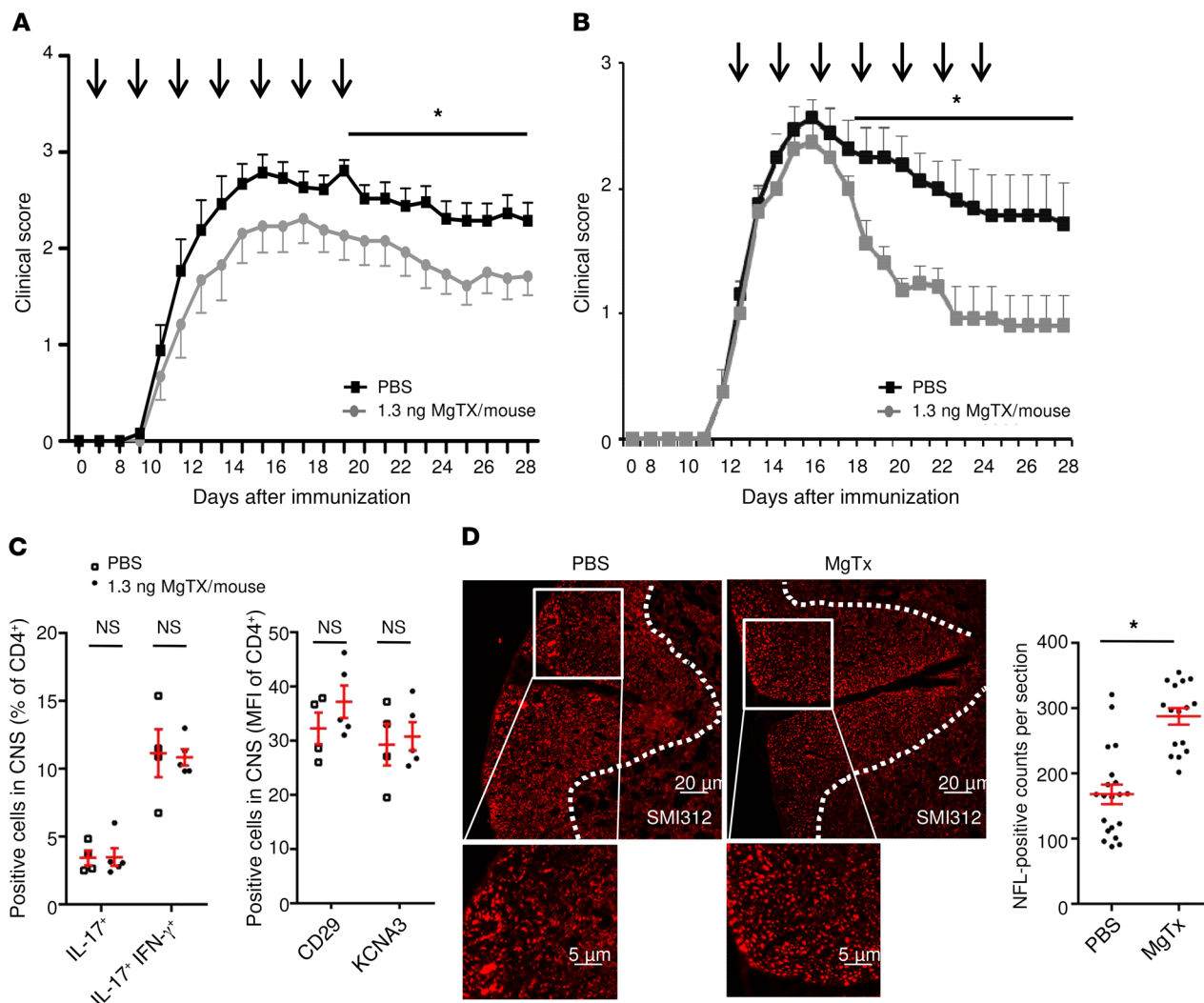


Figure 9. Intrathecal administration of MgTX ameliorates EAE disease course, and the differentiation of CNS-infiltrating 2D2 cells remains unchanged. (A) In mice with MOC₃₅₋₅₅-induced C57Bl6 EAE, intrathecal injection of MgTX (1.3 ng MgTX/mouse; $n = 11$ for 2 independent EAE experiments) into the CSF every other day for 14 days, starting on day 7, led to a significant and reproducible reduction in the clinical EAE score compared with the PBS-treated control group ($n = 13$). (B) In mice with MOC₃₅₋₅₅-induced C57Bl6 EAE, intrathecal injection of MgTX (1.3 ng MgTX/mouse, $n = 8$) into the CSF every other day for 14 days, starting after disease onset (treatment started when the EAE score was >1 , on approximately day 12), led to a significant reduction in the clinical EAE score compared with the PBS-treated control group ($n = 8$ for 2 independent EAE experiments). (C) Intracellular cytokine staining was performed on T lymphocytes ex vivo on day 28. Staining for IL-17 and IFN- γ was analyzed by flow cytometry and is shown as the percentage of CD4⁺ cells within the CNS and as the MFI of CD4⁺ cells. $n = 4$ PBS-treated mice; $n = 5$ MgTX-treated mice. (D) Cryosections of EAE mouse brains were stained for SMI312 ($n = 4$ –5 sections at least 100 μm apart, from 4 WT and MgTx-treated mice on day 28). Images were acquired using an Olympus microscope equipped with a cellSense camera and analyzed with ImageJ software. Scale bars: 20 μm and 5 μm (enlarged insets). Data indicate the mean \pm SEM. * $P < 0.05$, by multiple Student's t tests (A and B) or Mann-Whitney U test (C and D).

(Plano). Sections were incubated with 50 mM NH₄Cl in PBS and with blocking solution (0.5% fish gelatin (MilliporeSigma) and 0.1% OVA (MilliporeSigma) in PBS. Rabbit anti-L glutamate (Abcam) was diluted 1:250 in IgG-gold buffer (0.5% fish gelatin, 0.1% OVA, 0.01% Tween, 0.5 M NaCl in phosphate buffer) and incubated at 4°C for 60 hours. After washing, the secondary anti-rabbit-Fab conjugated to Nanogold (Nanoprobes) was applied to visualize the anti-L glutamate antibody, and the sections were silver enhanced. A Technai 12 transmission electron microscope (FE1, Thermo Fisher Scientific) was used for imaging. Quantification was performed for unstained control cells as well as unstimulated and stimulated Th17 cells.

Transfection of iGluSnFR and TeNT. Transfection of murine CD4⁺IL-17⁺ T cells was performed using a commercially available transfection kit (Nucleofector Kits for Mouse T Cells, VVPA-1006, Lonza) following the manufacturer's instructions. For each transfection, 3×10^6 CD4⁺IL-17⁺ T cells were transfected with 10–15 μg iGluSnFR or 10 μg TeNT/TeNT^{E234Q} via electroporation. Next, cells were incubated at 37°C for at least 24 hours and restimulated for 4 hours on an anti-CD3- and anti-CD28-coated plate. Cells were plated on poly-D-lysine-coated (PDL-coated) (10 $\mu\text{g}/\text{mL}$) wells and fixed with 4% PFA for 20 minutes. Image analysis was performed with Leica LAS-AF Lite software by looking at the mean pixel value of different regions of interest in the green channel.

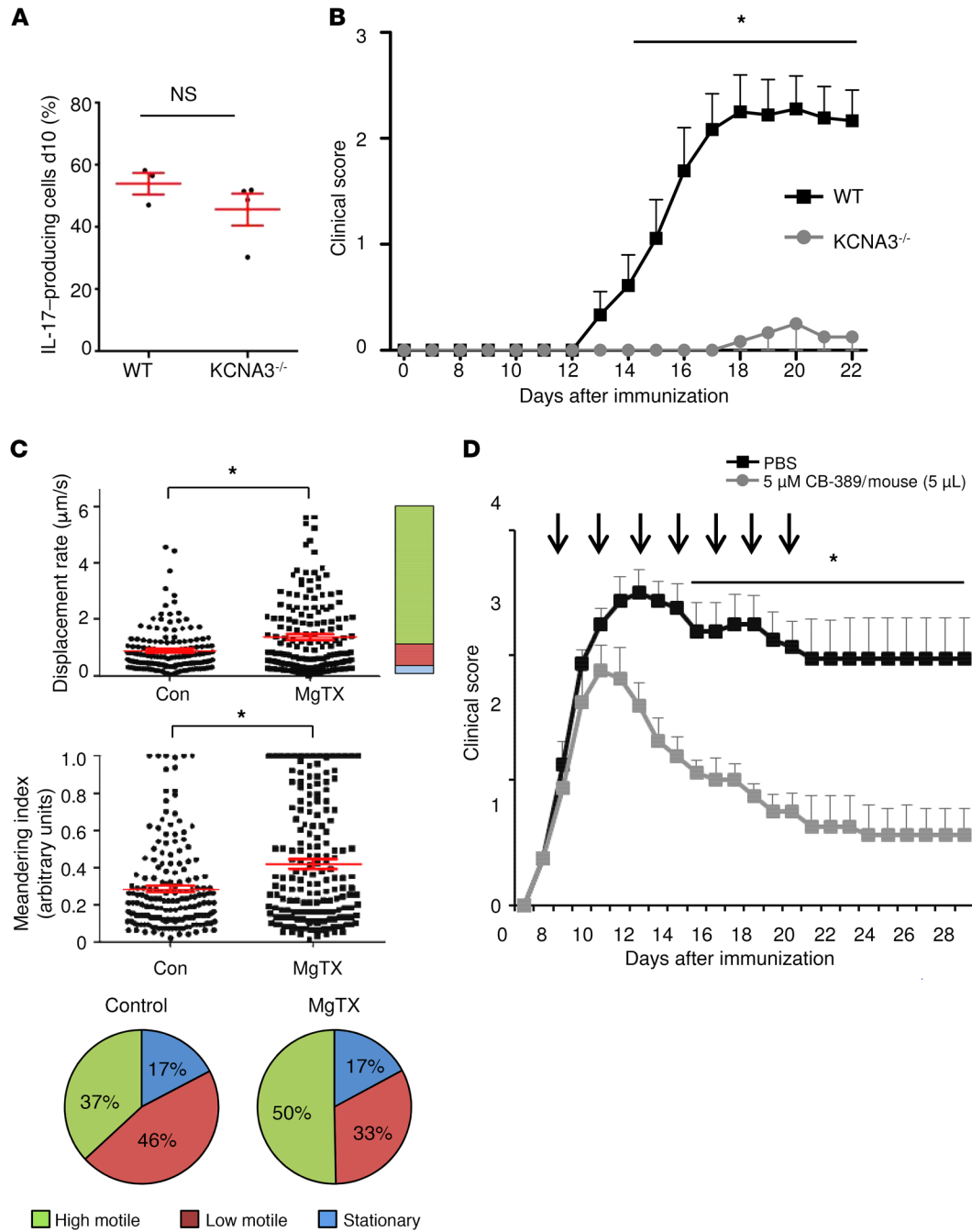


Figure 10. Intrathecal administration of glutaminase inhibitor CB-839 ameliorates disease course of EAE, and inhibition of $K_v1.3$ -mediated pathways modulates direct cell-cell contacts between T cells and neurons. (A) Intracellular staining of IL-17 in murine Th17 differentiated cells after 10 days TCR stimulation ($n = 6-7$). d10, day 10. (B) Passive cell transfer EAE with MOG-reactivated lymph node cells from KCNA3^{-/-} mice ($n = 6$) compared with EAE induction with MOG-reactivated lymph node cells from WT mice ($n = 9$ for 2 independent EAE experiments). (C) B6.2D2.RFP:Th17 cells were transferred into Rag^{-/-} mice to induce passive EAE. Two-photon microscopy was used to analyze T cell motility parameters of viable B6.2D2.RFP:Th17 cells before treatment ($n = 6$ mice; minimum of 30 T cells) and after MgTX treatment (5 μM; $n = 7$ mice; minimum of 30 T cells). The treatment was locally applied onto the brainstem. Stationary cells were defined by a displacement rate below 0.3 μm/s, low-motility cells reached displacement rates up to less than 0.8 μm/s, and high-motility cells had a displacement rate above 0.8 μm/s. (D) In MOG₃₅₋₅₅-induced C57BL/6 EAE mice, intrathecal injection of CB-839 (5 μM in 5 μL/mouse, $n = 8$) into the CSF every other day for 14 days, starting on day 7, led to a significant reduction in the clinical EAE score compared with the PBS-treated control group ($n = 8$ for 2 independent EAE experiments). Data indicate the mean ± SEM. * $P < 0.05$, by multiple Student's t tests (B and D) or Mann-Whitney U test (A and C).

Transfection efficacy for iGluSnFR was $64\% \pm 3\%$ as assessed by flow cytometric staining controls.

Statistics. Statistical analyses were performed with SPSS version 23 (IBM Corporation) and GraphPad Prism, version 6 (GraphPad Software) using a K-S test for normality, followed by a Mann-Whitney *U* test, an unpaired, 2-tailed Student's *t* test, or a 1-way ANOVA followed by Dunnett's or Tukey's test post hoc test for multiple comparisons, as appropriate. Spearman's rank correlation test was performed for non-normally distributed data. Data are presented as the mean \pm SEM unless otherwise indicated. A *P* value of less than 0.05 was considered statistically significant.

Study approval. All animal experiments were approved by the Landesuntersuchungsamt Rheinland-Pfalz (Koblenz, Germany) and conducted according to German laws for the protection of animals. Experiments involving human cell cultures were approved by the local ethics committee (Landesaerztekammer Rheinland-Pfalz) and performed in accordance with Declaration of Helsinki principles. All patients provided written informed consent.

Author contributions

KB, FZ, and SB conceived the study. KB, BW, CT, LB, TR, DL, KP, SS, EMKA, AS, and SGM performed experiments and analyzed data. KB, FZ, and SB wrote and edited the manuscript.

Acknowledgments

This study was supported by the Deutsche Forschungsgemeinschaft (DFG) (SFB CRC-TR-128, to FZ and SB; CRC-1080, to FZ; SFB 1292, to FZ; and BI1822/1-1, to SB) and the Gemeinnützige Hertie-Stiftung (mylab 2017, to SB). The authors thank Heike Ehrengard, Ilse Graevenitz, Silke Fregin, Andreas Zymny, Christin Liefänder, Birgit Hohmann, and Jerome Birkenstock for their excellent technical assistance and Cheryl Ernest and Rosie Gilchrist for editing the manuscript.

Address correspondence to: Frauke Zipp or Stefan Bittner, Langenbeckstraße 1, Building 308, 55131 Mainz, Germany. Phone: 49.0.6131.17.7156; Email: zipp@uni-mainz.de (F. Zipp) or bittner@uni-mainz.de (S. Bittner).

- Levite M. Glutamate, T cells and multiple sclerosis. *J Neural Transm (Vienna)*. 2017;124(7):775–798.
- Luchtman D, et al. In vivo and in vitro effects of multiple sclerosis immunomodulatory therapeutics on glutamatergic excitotoxicity. *J Neurochem*. 2016;136(5):971–980.
- Rajda C, Pukoli D, Bende Z, Majláth Z, Vécsei L. Excitotoxins, Mitochondrial and Redox Disturbances in Multiple Sclerosis. *Int J Mol Sci*. 2017;18(2):E353.
- Macrez R, Stys PK, Vivien D, Lipton SA, Docagne F. Mechanisms of glutamate toxicity in multiple sclerosis: biomarker and therapeutic opportunities. *Lancet Neurol*. 2016;15(10):1089–1102.
- Kostic M, Zivkovic N, Stojanovic I. Multiple sclerosis and glutamate excitotoxicity. *Rev Neurosci*. 2013;24(1):71–88.
- Sarchielli P, Greco L, Floridi A, Floridi A, Gallai V. Excitatory amino acids and multiple sclerosis: evidence from cerebrospinal fluid. *Arch Neurol*. 2003;60(8):1082–1088.
- Schubert D, Piasecki D. Oxidative glutamate toxicity can be a component of the excitotoxicity cascade. *J Neurosci*. 2001;21(19):7455–7462.
- Hohlfeld R, Kerschensteiner M. Antigliamatergic therapy for multiple sclerosis? *Lancet Neurol*. 2016;15(10):1003–1004.
- Friese MA, Schattling B, Fugger L. Mechanisms of neurodegeneration and axonal dysfunction in multiple sclerosis. *Nat Rev Neurol*. 2014;10(4):225–238.
- Garg SK, Banerjee R, Kipnis J. Neuroprotective immunity: T cell-derived glutamate endows astrocytes with a neuroprotective phenotype. *J Immunol*. 2008;180(6):3866–3873.
- Melzer N, et al. Excitotoxic neuronal cell death during an oligodendrocyte-directed CD8⁺ T cell attack in the CNS gray matter. *J Neuroinflammation*. 2013;10:121.
- Siffrin V, et al. In vivo imaging of partially reversible th17 cell-induced neuronal dysfunction in the course of encephalomyelitis. *Immunity*. 2010;33(3):424–436.
- Newsholme P. Why is L-glutamine metabolism important to cells of the immune system in health, postinjury, surgery or infection? *J Nutr*. 2001;131(9 Suppl):2515S–22S; discussion 2523S.
- Nakaya M, et al. Inflammatory T cell responses rely on amino acid transporter ASCT2 facilitation of glutamine uptake and mTORC1 kinase activation. *Immunity*. 2014;40(5):692–705.
- Metzler B, Gfeller P, Guinet E. Restricting glutamine or glutamine-dependent purine and pyrimidine syntheses promotes human T cells with high FOXP3 expression and regulatory properties. *J Immunol*. 2016;196(9):3618–3630.
- Klysz D, et al. Glutamine-dependent α -ketoglutarate production regulates the balance between T helper 1 cell and regulatory T cell generation. *Sci Signal*. 2015;8(396):ra97.
- Legroux L, Arbour N. Multiple Sclerosis and T Lymphocytes: An Entangled Story. *J Neuroimmune Pharmacol*. 2015;10(4):528–546.
- Codarri L, Greter M, Becher B. Communication between pathogenic T cells and myeloid cells in neuroinflammatory disease. *Trends Immunol*. 2013;34(3):114–119.
- Waisman A, Hauptmann J, Regen T. The role of IL-17 in CNS diseases. *Acta Neuropathol*. 2015;129(5):625–637.
- Cua DJ, et al. Interleukin-23 rather than interleukin-12 is the critical cytokine for autoimmune inflammation of the brain. *Nature*. 2003;421(6924):744–748.
- Langrish CL, et al. IL-23 drives a pathogenic T cell population that induces autoimmune inflammation. *J Exp Med*. 2005;201(2):233–240.
- Komiyama Y, et al. IL-17 plays an important role in the development of experimental autoimmune encephalomyelitis. *J Immunol*. 2006;177(1):566–573.
- Sie C, Korn T, Mitsdoerffer M. Th17 cells in central nervous system autoimmunity. *Exp Neurol*. 2014;262 Pt A:18–27.
- Kebr H, et al. Human TH17 lymphocytes promote blood-brain barrier disruption and central nervous system inflammation. *Nat Med*. 2007;13(10):1173–1175.
- Lopes Pinheiro MA, et al. Immune cell trafficking across the barriers of the central nervous system in multiple sclerosis and stroke. *Biochim Biophys Acta*. 2016;1862(3):461–471.
- Williams PR, et al. A recoverable state of axon injury persists for hours after spinal cord contusion in vivo. *Nat Commun*. 2014;5:5683.
- Criste G, Trapp B, Dutta R. Axonal loss in multiple sclerosis: causes and mechanisms. *Handb Clin Neurol*. 2014;122:101–113.
- Grigoriadis N, van Pesch V, ParadigMS Group. A basic overview of multiple sclerosis immunopathology. *Eur J Neurol*. 2015;22 Suppl 2:3–13.
- Baker D, Marta M, Pryce G, Giovannoni G, Schmierer K. Memory B Cells are Major Targets for Effective Immunotherapy in Relapsing Multiple Sclerosis. *EBioMedicine*. 2017;16:41–50.
- Cebrián C, et al. MHC-I expression renders catecholaminergic neurons susceptible to T-cell-mediated degeneration. *Nat Commun*. 2014;5:3633.
- Vagaska B, et al. MHC-class-II are expressed in a subpopulation of human neural stem cells in vitro in an IFN γ -independent fashion and during development. *Sci Rep*. 2016;6:24251.
- Pattu V, et al. SNARE protein expression and localization in human cytotoxic T lymphocytes. *Eur J Immunol*. 2012;42(2):470–475.
- Das V, et al. Activation-induced polarized recycling targets T cell antigen receptors to the immunological synapse; involvement of SNARE complexes. *Immunity*. 2004;20(5):577–588.
- McMahon HT, et al. Cellubrevin is a ubiquitous tetanus-toxin substrate homologous to a putative synaptic vesicle fusion protein. *Nature*. 1993;364(6435):346–349.
- Feske S, Wulff H, Skolnik EY. Ion channels in innate and adaptive immunity. *Annu Rev Immunol*. 2015;33:291–353.
- Bittner S, et al. TASK1 modulates inflammation and neurodegeneration in autoimmune inflam-

- mation of the central nervous system. *Brain*. 2009;132(Pt 9):2501-2516.
37. Grishkan IV, Tosi DM, Bowman MD, Harary M, Calabresi PA, Gocke AR. Antigenic stimulation of Kv1.3-deficient Th cells gives rise to a population of Foxp3-independent T cells with suppressive properties. *J Immunol*. 2015;195(4):1399-1407.
 38. Kasatkina LA. 4-Aminopyridine sequesters intracellular Ca²⁺ which triggers exocytosis in excitable and non-excitable cells. *Sci Rep*. 2016;6:34749.
 39. Marvin JS, et al. An optimized fluorescent probe for visualizing glutamate neurotransmission. *Nat Methods*. 2013;10(2):162-170.
 40. Chandy KG, Norton RS. Peptide blockers of K_v1.3 channels in T cells as therapeutics for autoimmune disease. *Curr Opin Chem Biol*. 2017;38:97-107.
 41. Levite M, et al. Extracellular K(+) and opening of voltage-gated potassium channels activate T cell integrin function: physical and functional association between Kv1.3 channels and beta1 integrins. *J Exp Med*. 2000;191(7):1167-1176.
 42. Artym VV, Petty HR. Molecular proximity of Kv1.3 voltage-gated potassium channels and beta(1)-integrins on the plasma membrane of melanoma cells: effects of cell adherence and channel blockers. *J Gen Physiol*. 2002;120(1):29-37.
 43. Huppert J, et al. Cellular mechanisms of IL-17-induced blood-brain barrier disruption. *FASEB J*. 2010;24(4):1023-1034.
 44. Patel DD, Kuchroo VK. Th17 cell pathway in human immunity: lessons from genetics and therapeutic interventions. *Immunity*. 2015;43(6):1040-1051.
 45. Cahalan MD, Chandy KG. The functional network of ion channels in T lymphocytes. *Immunol Rev*. 2009;231(1):59-87.
 46. Scimemi A, Beato M. Determining the neurotransmitter concentration profile at active synapses. *Mol Neurobiol*. 2009;40(3):289-306.
 47. Bittner S, Meuth SG. Targeting ion channels for the treatment of autoimmune neuroinflammation. *Ther Adv Neurol Disord*. 2013;6(5):322-336.
 48. Zhu J, Yan J, Thornhill WB. The Kv1.3 potassium channel is localized to the cis-Golgi and Kv1.6 is localized to the endoplasmic reticulum in rat astrocytes. *FEBS J*. 2014;281(15):3433-3445.
 49. Beeton C, et al. Selective blockade of T lymphocyte K(+) channels ameliorates experimental autoimmune encephalomyelitis, a model for multiple sclerosis. *Proc Natl Acad Sci U S A*. 2001;98(24):13942-13947.
 50. Lu R, Schmidtke A. Direct intrathecal drug delivery in mice for detecting in vivo effects of cGMP on pain processing. *Methods Mol Biol*. 2013;1020:215-221.
 51. Polman CH, et al. Diagnostic criteria for multiple sclerosis: 2010 revisions to the McDonald criteria. *Ann Neurol*. 2011;69(2):292-302.
 52. Livak KJ, Schmittgen TD. Analysis of relative gene expression data using real-time quantitative PCR and the 2(-Delta Delta C(T)) method. *Methods*. 2001;25(4):402-408.
 53. Siffrin V, et al. Differential immune cell dynamics in the CNS cause CD4⁺ T cell compartmentalization. *Brain*. 2009;132(Pt 5):1247-1258.
 54. Herz J, Zipp F, Siffrin V. Neurodegeneration in autoimmune CNS inflammation. *Exp Neurol*. 2010;225(1):9-17.
 55. Mank M, et al. A genetically encoded calcium indicator for chronic in vivo two-photon imaging. *Nat Methods*. 2008;5(9):805-811.
 56. Geiger A, et al. Correlating calcium binding, Förster resonance energy transfer, and conformational change in the biosensor TN-XXL. *Biophys J*. 2012;102(10):2401-2410.
 57. Wolfrum U, Schmitt A. Rhodopsin transport in the membrane of the connecting cilium of mammalian photoreceptor cells. *Cell Motil Cytoskeleton*. 2000;46(2):95-107.